Porosity distribution in cyclic dolomites of the Lower Qiulitag Group (Upper Cambrian) in northwestern Tarim Basin, China

Yan-qiu Zhang, Zeng-hui Guo, Dai-zhao Chen

Citation: Yan-qiu Zhang, Zeng-hui Guo, Dai-zhao Chen, 2020. Porosity distribution in cyclic dolomites of the Lower Qiulitag Group (Upper Cambrian) in northwestern Tarim Basin, China, China Geology, 3, 425-444. doi: 10.31035/cg2020026.

View online: https://doi.org/10.31035/cg2020026

China Geology 3 (2020) 425−444

China Geology

Journal homepage: http://chinageology.cgs.cn
https://www.sciencedirect.com/journal/china-geology

Porosity distribution in cyclic dolomites of the Lower Qiulitag Group (Upper Cambrian) in northwestern Tarim Basin, China

Yan-qiu Zhang[a, c], Zeng-hui Guo[b], Dai-zhao Chen[b,*]

[a] *Development and Research Center of China Geological Survey, Ministry of Natural Resources, Beijing* 100037, *China*
[b] *Key Laboratory of Petroleum Resources Research, Institute of Geology and Geophysics, Chinese Academy of Sciences, Beijing* 100029, *China*
[c] *Institute of Earth and Environmental Science, University of Potsdam, Karl-Liebknecht-Str.* 24-25, 14476 *Potsdam-Golm, Germany*

ARTICLE INFO

Article history:
Received 26 March 2020
Received in revised form 14 May 2020
Accepted 2 July 2020
Available online 18 August 2020

Keywords:
Dolomites
Porosity
Cyclicity
Upper Cambrian
Stromatolite
Microbial build up
Oil-gas basin
Oil-gas exploration engineering
Tarim Basin
China

ABSTRACT

Increasing interests in hydrocarbon resources at depths have drawn greater attentions to the deeply-buried carbonate reservoirs in the Tarim Basin in China. In this study, the cyclic dolomite rocks of Upper Cambrian Lower Qiulitag Group from four outcrop sections in northwestern Tarim Basin were selected to investigate and evaluate the petrophysical properties in relation to depositional facies and cyclicity. The Lower Qiulitag Group includes ten lithofacies, which were deposited in intermediate to shallow subtidal, restricted shallow subtidal, intertidal, and supratidal environments on a carbonate ramp system. These lithofacies are vertically stacked into repeated shallowing-upward, meter-scale cycles which are further grouped into six third-order depositional sequences (Sq1 to Sq6). There are variable types of pore spaces in the Lower Qiulitag Group dolomite rocks, including interparticle, intraparticle, and fenestral pores of primary origin, inter crystal, and vuggy pores of late diagenetic modification. The porosity in the dolomites is generally facies-selective as that the microbially-originated thrombolites and stromatolites generally yield a relatively high porosity. In contrast, the high-energy ooidal grainstones generally have very low porosity. In this case, the microbialite-based peritidal cycles and peritidal cycle-dominated highstand (or regressive) successions have relatively high volumes of pore spaces, although highly fluctuating (or vertical inhomogeneous). Accordingly, the grainstone-based subtidal cycles and subtidal cycle-dominated transgressive successions generally yield extremely low porosity. This scenario indicates that porosity development and preservation in the thick dolomite successions are primarily controlled by depositional facies which were influenced by sea-level fluctuations of different orders and later diagenetic overprinting.

1. Introduction

The Tarim Basin is prolific in hydrocarbon resources in western China. In recent two decades, a number of oil and gas fields were discovered in the Cambrian-Ordovician carbonate successions (Li DS et al., 1996; Chen ZQ and Shi GR, 2003; Zheng HR et al., 2007; Yang YJ and Liu JD, 2011; Zheng JF et al., 2015; Zhang ZY et al., 2018). As estimated, abundant hydrocarbon resources are still reserved in the Lower Paleozoic carbonate successions in Tarim Basin (Zheng HR et al., 2007; Huang HP et al., 2016), which will become the potential targets for future exploration. Previous geological and seismic investigations have shown that dolomite rocks of the Lower Paleozoic, particularly of the Cambrian extensively occur subsurface and are generally buried deeply (generally >8 km) in the basin (Zhang JT et al., 2008; Zhu DY et al., 2015). Therefore, a detailed analysis of the spatial petrophysical variations in the outcrop dolomites based on different scales from lithofacies to third-order sequence framework can provide a useful analogue to understand the porosity distribution of equivalent deeply-buried dolomites subsurface in Tarim Basin, facilitating constructing reservoir model and predicting favourable reservoirs subsurface there.

Numerous studies have explored the causes (or controls) on which the pores were developed and distributed in dolomite rocks (Lucia F and Major R, 1994; Purser B et al., 1994; Saller AH and Henderson N, 1998; Saller AH et al.,

First author: *E-mail address*: zhyq1998@126.com (Yan-qiu Zhang)..

* Corresponding author: *E-mail address*: dzh-chen@mail.iggcas.ac.cn (Dai-zhao Chen).

doi:10.31035/cg2020026
2096-5192/© 2020 China Geology Editorial Office.

2001). In general, many factors are controlling the pore development and distribution in dolomites, such as the primary sediment texture and mineralogy, subaerial emergence and penetration of meteoric water, distance below the emergent surface, duration of subaerial exposure, degrees of early cementation and early diagenesis (James NP and Choquette PW, 1984; Saller AH et al., 1994; Dickson J and Saller AH, 1995). Notably, these factors are closely related to the fluctuation of relative sea level by influencing the patterns of depositional facies and the development of carbonate cycles and sequences. Owe to the accidental and inevitable fluctuations, the porosity distribution is distinctive in carbonates (Sarg J, 1988; Goldhammer R et al., 1990; Read J and Horbury AD, 1993; Saller AH et al., 1999b).

In Tarim Basin, the relationship between porosity distribution and sedimentary sequences (e.g. second-order sequence) in Cambrian carbonates has been investigated recently (Yu BS et al., 2005; Fan TL et al., 2007; Liu JD et al., 2009; Chen YQ et al., 2010; Xiao ZH et al., 2011). However, detailed relationships of porosity with lithofacies, cycles (parasequences), and third-order sequences have not yet been disclosed. Importantly, the Lower Qiulitag Group is characterized by cyclic dolomites (Zhang YQ et al., 2015), providing a great opportunity to explore their relationships. Thus, this study aims to characterize the porosity distribution in the facies, meter-scale cycles and associated third-order sequences of the Lower Qiulitag Group in NW Tarim Basin, to figure out their relationships and discover the factors controlling the porosity development in the cyclic carbonate platform. The study is expected to provide important implications in understanding the distributions of hydrocarbon in dolostone reservoirs.

2. Geological setting

The Tarim Basin, located in the southern part of the Xinjiang Autonomous Region in northwest China, is a cratonic basin bordered by the Tianshan Mountains to the north, the Kunlun Mountains to the southwest and the Algyn Mountains to the southeast (Fig. 1). It is filled by Precambrian-Permian marine sedimentary successions and Mesozoic-Cenozoic non-marine successions (Li DS et al., 1996; Jia CZ and Wei GQ, 2002). This large sedimentary basin has been subjected to multiphase tectonic activities, including Caledonian, Hercynian, Indosinian and Himalayan events (Kang YZ and Kang ZH, 1996; Jia CZ, 1997; Tang LJ, 1997), which influences not only the development of this basin but also the evolution and distribution of hydrocarbon. Along the ENE-trending Bachu-Keping-Asku Uplift in the northwest flank of the basin, the Precambrian to Permian rocks, however, were subject to extensive uplift and subsequent exhumation due to collision of the Tarim plate and Tianshan island arc to the north from the Mesozoic onwards (Zhang SB and Gao QQ, 1992; Kang YZ and Kang ZH, 1996; Zhou ZY, 2001; Jia CZ et al., 2004). A marine carbonate platform developed during Cambrian and Ordovician in this region, as a result of high-frequency sea-level fluctuations (Gu JY, 2000; Cai C et al., 2001; Zheng HR et al., 2007). The Cambrian successions are mainly characterized by tidal, restricted platform, open platform, and platform-margin marls, mudstones and carbonates/evaporates in western Tarim Basin (Kang YZ and Kang ZH, 1996; Feng ZZ et al., 2007; Yang YJ and Liu JD, 2011). The Cambrian successions

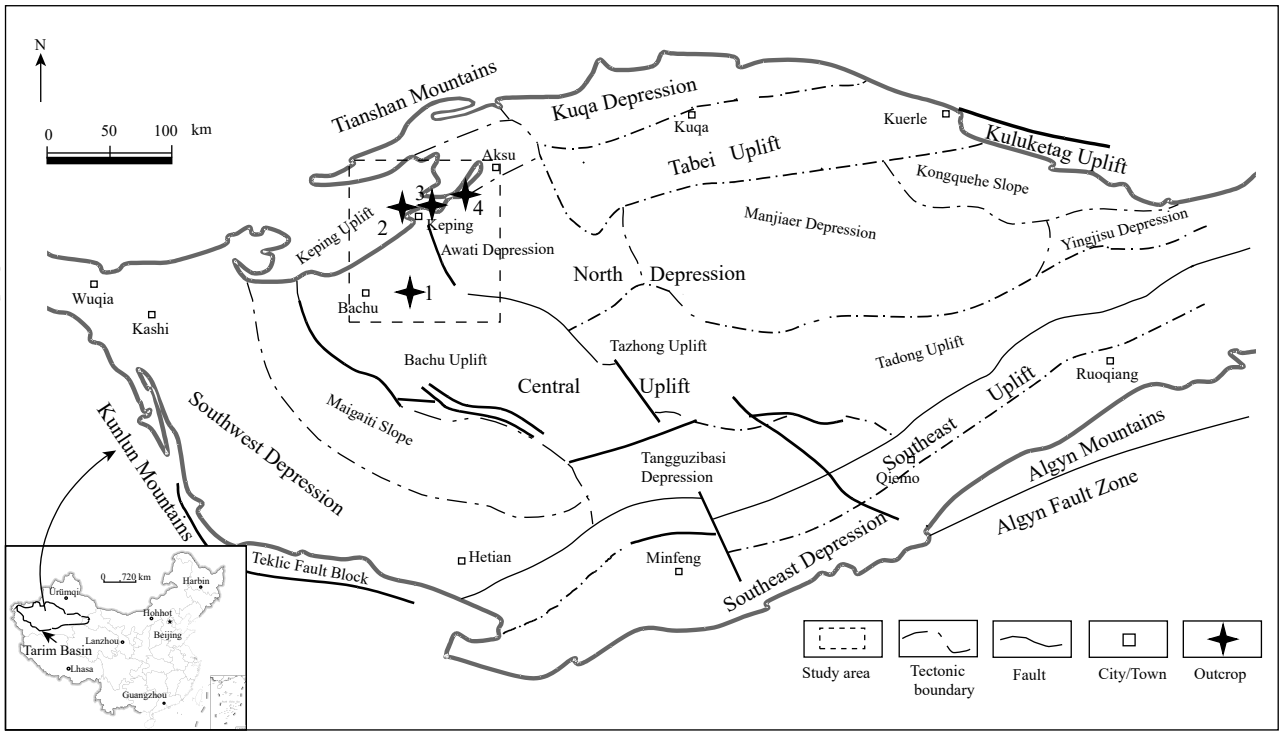

Fig. 1. Location of the study area and general structural units in the Tarim Basin (modified from Lin CS et al., 2011). 1−Yong'anba section (YAB); 2−Keping section (KP); 3−Tonggusibulong section (TGL); 4−Penglaiba section (PLB).

consist of six lithological formations, including the Yurtus, Xiaoerbulak, Wusongger, Shayilik, Awatag Formations and Lower Qiulitag Group in an ascending order, which are overwhelmingly composed of dolomites except for bedded phosphatic chert and black shale succession in the lowermost Cambrian Yurtus Formation (Zhou XQ et al., 2014; Zhou XQ et al., 2015). Among them, the Lower Qiulitag Group of Upper Cambrian is the studied interval, which overlies the Awatag Formation dolomites containing evaporites and redbeds (Fig. 2; Zhang YQ et al., 2015), and is covered by the Lower Ordovician dolostone-limestone interbeds (Zhou ZY, 2001; Shao LW et al., 2002; Jia CZ et al., 2004; Cai XY et al., 2009; Guo C et al., 2018a, 2018b, 2020). The Lower Qiulitag Group was deposited on a gentle slope, restricted shallow subtidal ramp and localized shoal and lagoonal environments, which is characterized by thick cyclic dolomites with dominant microbialite (thrombolite, stromatolite) in the lower portion and microbial boundstone and oolite in the upper part.

3. Sampling methodology

Four outcrop sections exposing the Lower Qiulitag Group were measured and logged bed by bed at Penglaiba (PLB) in Aksu City, Tonggusibulong (TGL) and Keping (KP) in Keping County and Yong ’anba (YAB) in Bachu County, western Tarim Basin (Fig. 1). Of them, the PLB section, 297 m thick, has the most complete outcrop the Lower Qiulitag Group. The TGL section of the Lower Qiulitag Group, 761 m thick, is well exposed in Keping area. YAB (64 m thick) and KP (96 m thick) sections, however, only are exposed to the upper part of Lower Qiulitag Group.

Hundreds of fresh hand samples and thin sections were examined to distinguish individual lithofacies and reveal depositional environments. High-frequency, meter-scale cycles were identified mainly based on the recurrences of vertically-stacked lithofacies (or facies) and their transitional (gradual or abrupt) patterns across the bounding surfaces. Third-order sequences were determined based on the cycle stacking patterns and accommodation changes revealed by Fischer plots (Fischer AG, 1964; Goldhammer RK et al., 1987; Read J and Goldhammer R, 1988; Osleger D and Read JF, 1993; Chen DZ et al., 2001; Chen DZ and Tucker ME, 2003; Guo C et al., 2018b), together with facies stacking patterns (i.e. percentages of peritidal facies in each cycle) and depositional indicators.

In further, fifty-nine plugs drilled from outcrops were measured for porosity and permeability by gas porosimetry. Depending on their lithofacies type and cycle position, 194 thin sections were further impregnated by blue/red epoxy for determining porosity by point counting. Standard petrographic microscopy was used to observe the thin sections. The dolomite texture in this study was classified after Sibley DF and Gregg JM (1987), and the porosity was defined after Choquette PW and Pray LC (1970).

This study is a continuation of the former research published by Zhang YQ et al. (2015), where the lithofacies,

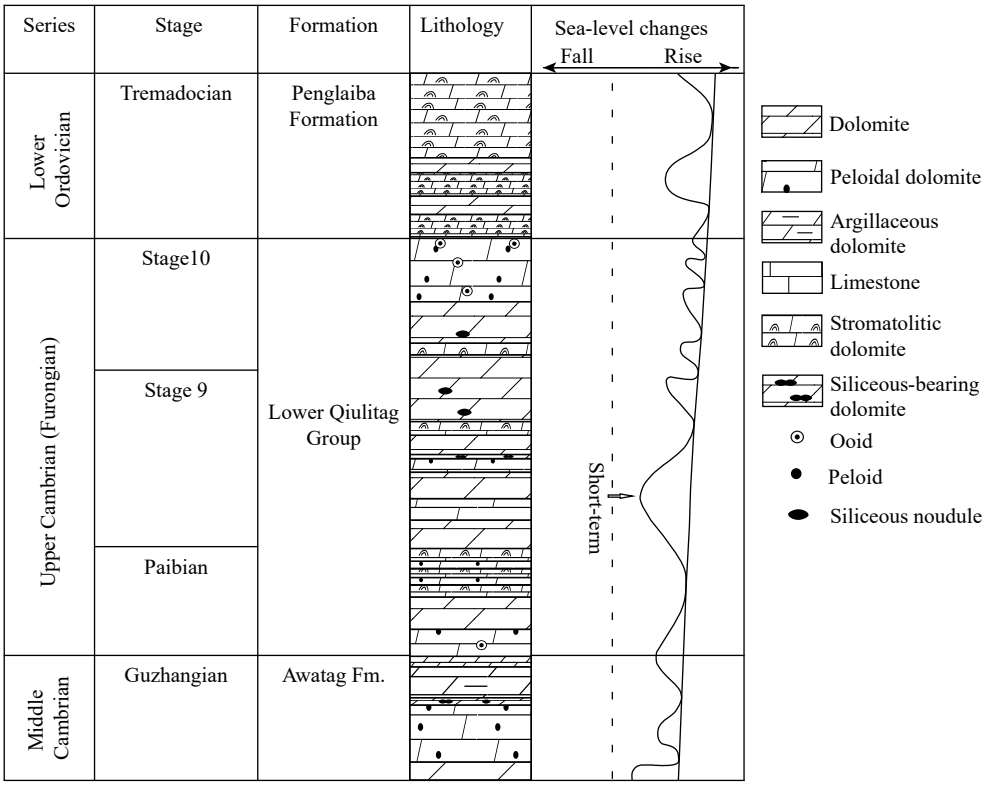

Fig. 2. Stratigraphic system of Cambrian in the northwestern Tarim Basin, mainly based on the data from references (Zhou ZY et al., 1990; Zhang SB and Gao QQ, 1992; Zhou LK et al., 1991; Zhou ZY, 2001). Sea-level curve from the publications by Haq BU and Schutter SR, 2008, Zhang YQ et al., 2015.

cycles, and sequences of the Lower Qiulitag Group had been described and interpreted in detail.

4. Facies and cyclicity

4.1. Facies

The Upper Cambrian Lower Qiulitag Group in the study area is overwhelmingly composed of cyclic dolomites, which are interpreted to have been deposited in intermediate to shallow subtidal, to restricted shallow subtidal, to intertidal and supratidal environments on a carbonate ramp system (Fig. 3; Zhang YQ et al., 2015). Ten main lithofacies (L1−L10) are identified based on lithology and sedimentary structures. Detailed descriptions are listed in Table 1.

Intertidal to supratidal facies includes thin laminite (L1), thick laminite (L2; Figs. 4a– b), wavy laminite (L3), and stromatolite (L4; Figs. 4c– d), which predominate over the lower-middle part of the Lower Qiulitag Group. Typically, these lithofacies stack vertically into a meter-scale conformable succession from L4 to L1. Restricted shallow subtidal to deep intertidal facies mainly include stratiform thrombolite (L5; Figs. 4e–f), cross-bedded pisolitic grainstone (L6), and thin-bedded ribbon (wavy) mudstone to packstone (L7). Vertically, L5 is commonly overlain by L4 and/or L2/L3 (Fig. 5a) in a vertical conformable succession (Fig. 3). In some cases, L6 is underlain by L7 (Fig. 3C) which generally shows wavy and ribbon-like stratification.

These lithofacies mainly occur in the lower-middle part of the Lower Qiulitag Group. Open marine subtidal facies mainly includes thick- to massively bedded oolite (L8; Figs. 5d, f, 6a –b), microbial buildup (L9; Figs. 5d, 6c –e) and lenticular to platy dolomite (L10; Figs. 5d, 6f), which largely distribute in the mid-upper part of the Lower Qiulitag Group. L8 is rarely overlain by intertidal to supratidal facies (L1 to L3), and commonly overlies, but locally co-occurs laterally with L9. In places, L8 is underlain by L10 within vertical meter-scale conformable successions (Fig. 3).

4.2. Meter-scale cycles and sequences

In general, the depositional facies are vertically arranged into hundreds of shallowing-upward, meter-scale cycles in the Lower Qiulitag Group. These cycles are commonly composed of a thin basal horizon reflecting abrupt deepening, and a

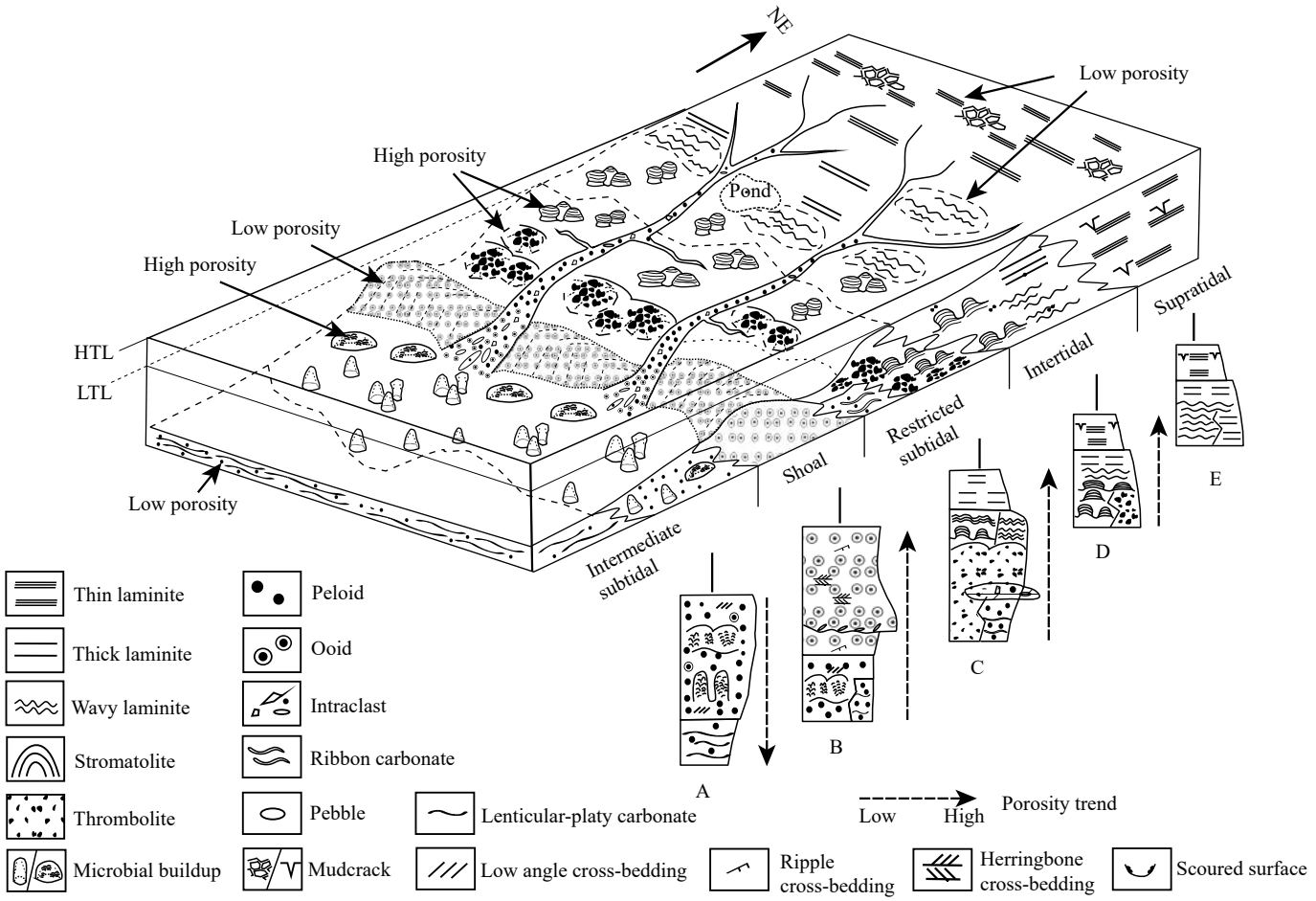

Fig. 3. Schematic facies model of a carbonate ramp system in the study area (modified from Zhang YQ et al., 2015). A−E−show the meter-scale depositional successions (or cycles) in different environments, from supratidal, to intertidal, to restricted shallow subtidal, and shoals and intermediate subtidal facies. The high porosity is present in stromatolite (L4), thrombolite (L5), cross-bedded packstone/grainstone lentil (L6) and microbial buildup (L9), while low porosity is generally present in thin laminites (L1), wavy laminites (L3), ribbon dolomites (L7), oolites (L8) and lenticular to platy dolomites (L10). LTL−low tidal level; HTL−high tidal level.

thicker upper succession showing gradual shallowing upwards. Peritidal and shallow subtidal cycle are further identified. The peritidal cycles commence with shallow subtidal to intertidal facies (lithofacies L5 to L2) and are capped by inter-supratidal facies (lithofacies L3 to L1; Fig. 3), which are dominant in the lower-middle of the studied intervals. Of these, the thrombolite-based peritidal cycle is the most common and comprises basal L5 facies, typically followed by L4 through L1 upwards. In contrast, shallow subtidal cycles are commonly composed of deep to intermediate subtidal facies (e.g. lithofacies L10) at their bases passing up into shallow subtidal facies (e.g. lithofacies L8 or L9), which mainly occur in the upper part of studied successions (Zhang YQ et al., 2015).

Six third-order depositional sequences (Sq1 to Sq6) are distinguished according to outcrop investigations, variations

Table 1. Characteristics of lithofacies in dolomites of the Lower Qiulitag Group in NW Tarim Basin, China.

Lithofacies/ Thickness	Lithology	Description	Occurrence	Depositional environment	Porosity
Intertidal to supratidal					
Thin laminite (L1)(0.1–0.6 m)	Alternating Ms with peloidal Ws/Ps, minor well-sorted, and rounded quartz silts disseminated	Light grey to grey, yellowish to reddish locally. Thin- to medium-bedded; mm-scale laminae, parallel lamination, flake pebbles intercalated locally, mud cracks common, reddening coloration locally where lamination obscured. Micritic dolomite crystal is dominant	Common at four sections; caps of peritidal cycles	Less agitated upper intertidal to supratidal flats	Poor, 0.1% to 8.5%, mean 1.3%, general 0.1% to 1.0%; BC common and minor VUG partly filled by dolomite and calcite
Thick laminite (L2)(0.1–1.5 m)	Alternating Ms with peloidal Ps/Ws or microbialite	Light grey to dark grey, reddish locally. Thin- to thick-bedded; cm-scale parallel to subparallel laminae, microbial fabrics intercalated locally, intraclasts pebbles, rare mud cracks, and silica bands/nodules; microbial or cryptomicrobial elements common. Fine dolomite crystal in the matrix, dirty anhedral crystal dominant	Common on the mid-upper part of PLB; abundant at TGL; minor on the top part of YAB; caps of peritidal cycles dominant, local bases of peritidal cycles	Low-energy upper intertidal to supratidal flats	Common, 1.0% to 12.5%, mean 4.7%; BC common and minor VUG partly filled with dolomite and calcite
Wavy laminite (L3)(0.1–2.0 m)	Alternating peloidal Ws/Ps with microbialites or intergrown microbialites	Grey to dark grey. Thin- to thick-bedded; mm- to cm-scale, mild undulatory laminae; domical stromatolites intercalated locally; minor siliceous nodules; microbes and/or cryptomicrobes dominant. Fine dolomite crystal in the matrix, dirty anhedral crystal dominant	Common at KP; less common at TGL and PLB; minor on the lower part of YAB; bases and caps of peritidal cycles	Low-energy intertidal to the lower supratidal flats	Poor, 0.1% to 4%, mean 1.9%; BC, VUG, and FR filled with dolomite and calcite
Stromatolite (L4)(0.1–2.0 m)	Intergrown microbialites and/or cryptomicrobialites	Grey to dark grey common. Medium- to thick-bedded; laterally-linked domical and/or hemispheroidal morphologies; smooth to convoluted microbial laminae; fenestral or irregular pores filled by later cement common; fenestral or irregular pores filled by later cements commonly. Micritic dolomite crystal is dominant	Common at PLB and TGL, rare at KP; caps of peritidal cycles	Restricted shallowest subtidal to intertidal setting	Relative rich, 0.1% to 12.5%, mean 6%, common between 3%–10%; FE, BC, BP, and VUG, partly filled with quartz, coarse dolomite, and bitumen
Restricted shallow subtidal to deep intertidal					
Stratiform thrombolite (L5)(0.2–2.2 m)	Thrombolitic microbialites or Bs.	Grey to dark grey. Medium- to massively-bedded, stratiform to mild hummocky configuration; mottled appearance (macrofabrics); clotted fabrics (mesoclots), complex internal microbial microfabrics, minor microbial filaments remained; abundant fenestrae and irregular pores filled by later cement. Micrited clots dominant	All four sections, abundant at PLB and TGL; common on the mid-upper part of YAB; rare at KP; bases of cycles	Restricted shallow subtidal to deep intertidal	Common, 0.1% to 15.0%, mean 4.9%; BP and VUGs common, minor FR, minor dissolution pores within calcite crystals, later dolomite, calcite, and quartz filling in most pores

Table 1. (*Continued*)

Lithofacies/ Thickness	Lithology	Description	Occurrence	Depositional environment	Porosity
Cross-bedded pisolitic Gs (L6)(0.2–0.5 m)	Pebbly peloidal/microbial Gs.	Grey to dark grey.Thin- to medium-bedded; lens-shaped beds intercalated in L5; erosive bases with lag flat pebbles common; microbial fragments. Micrited peloids (50–300 μm), very fine to fine anhedral dolomite crystal in the matrix	Less common at TGL, PLB, and KP; the lower-mid part of cycles	Intertidal creek on microbial mat or tidal washover	Relative rich, 1.8% to 16.5%, mean 7.5%; BC and BP common, minor WP, some bitumen filling in pores
Thin-bedded ribbon (wavy) dolomite (L7)(0.1–0.6 m)	Peloidal Ms to Ps.	Grey to dark grey. Thin-bedded; ribbon-like stratification with wavy to ripple cross-lamination; rare skeletal elements. Finely dolomite crystal (10–50 μm) in the matrix; micritic and fine dolomite in grains	Common at TGL, KP and PLB; bases of peritidal cycles	Restricted shallow subtidal environment	Less common, 0.1% to 8.2%, mean 2.7%; BC and VUG common, rare WP, some bitumen and quartz filling in pores
Open marine subtidal					
Oolite (L8)(0.3–6.5 m)	Peloidal-ooidal Gs and pebbly (or intraclasts) ooidal Gs common with a few skeletal grains	Light grey to dark grey. Medium- to thick-bedded even massively-bedded; well-sorted and grain-supported fabrics; cross-bedding, discontinuous wavy bedding; basal and internal erosive surfaces common with lag pebbles; structures and grain fabrics obscured commonly by postdepositional dolomitization and crystallization. Mainly fine-medium dolomite crystal in the matrix; micritic- and fine-crystal in grains	Common on the mid-upper part of KP; common at YAB; less common on the lower and upper parts of TGL; bases/caps of cycles	High-energy shallow subtidal sandy shoals and/or tidal channels	Less common, 0.1% to 20.0%, mean 3.1%; BC and VUG common, BP less common, minor WP, FR and dissolution pores, larger dolomite (saddle), calcite, quartz and bitumen partly filling in pores
Microbial buildups (L9)(1.0–10.0 m)	Microbial or thrombolitic Bs/Fs	Grey to dark grey. Thick-bedded to massively-bedded; discrete columnar morphologies, mounded forms with dendroid to digitate *in-situ* growth structure, minor microbial filaments preserved; co-occurrence with peloidal-ooidal Gs (L8); silicification common; microbes and/or cryptomicrobes dominant, *Girvanella*, *Renalcis* and *Epiphyton* locally; rare skeletal fossils. Fine-medium dolomite crystal in the matrix; micrited clots	Common on the mid-upper part of TGL; rare at YAB; mid-upper parts of subtidal cycles	Microbial buildups colonizing on subtidal sandy shoals or tidal channels	Common, 2.0% to 25.0%, mean 6.9%; BC and VUG common, channel and FR less common, larger dolomite, calcite, quartz and bitumen partly filling in pores
Lenticular to platy dolomite (L10)(0.1–1.0 m)	Peloidal Ws/Ps with minor ooids and a few skeletal grains, minor argillaceous matter	Grey to dark grey. Thin- to medium-bedded; lenticular to platy stratification with more or less argillaceous strips; trilobite, crinoids, and brachiopod locally. Fine-medium dolomite crystal in the matrix; micritic crystal in grains	Less common on upper parts of TGL; bases of subtidal cycles	Relatively deep (intermediate) subtidal environment	Common, 0.1% to 10.0%, mean 3.4%; BC and VUG common, minor FR and dissolution pores, coarse dolomite and quartz partly filling in pores

Notes: Ms–dolomudstone, Ws–dolowackestone, Ps–dolopackstone, Gs–dolograinstone, Bs–doloboundstone, Fs–doloframestone, BP–interpartical pore, WP–intrapartical pore, BC–intercrystal pore, FE–fenestral pore, VUG–vug, FR–fracture.

in cycle stacking patterns, and vertical facies variations. Sequence boundaries are generally gradational and conformable stratigraphic intervals, rather by a single surface. These third-order sequences can be further grouped into lower-order sequence sets: The lower and upper sequence sets (Figs. 7, 8). The lower sequence set (Sq1 to Sq3) is characterized by peritidal facies-predominated sequences and progressive decreases in accommodation space, indicating a

longer-term fall in sea level. In contrast, the upper sequence set (Sq4 to Sq6) is characterized by subtidal facies-dominated sequences and progressive increases in accommodation space, indicating a longer-term rise in sea level. The transgressive

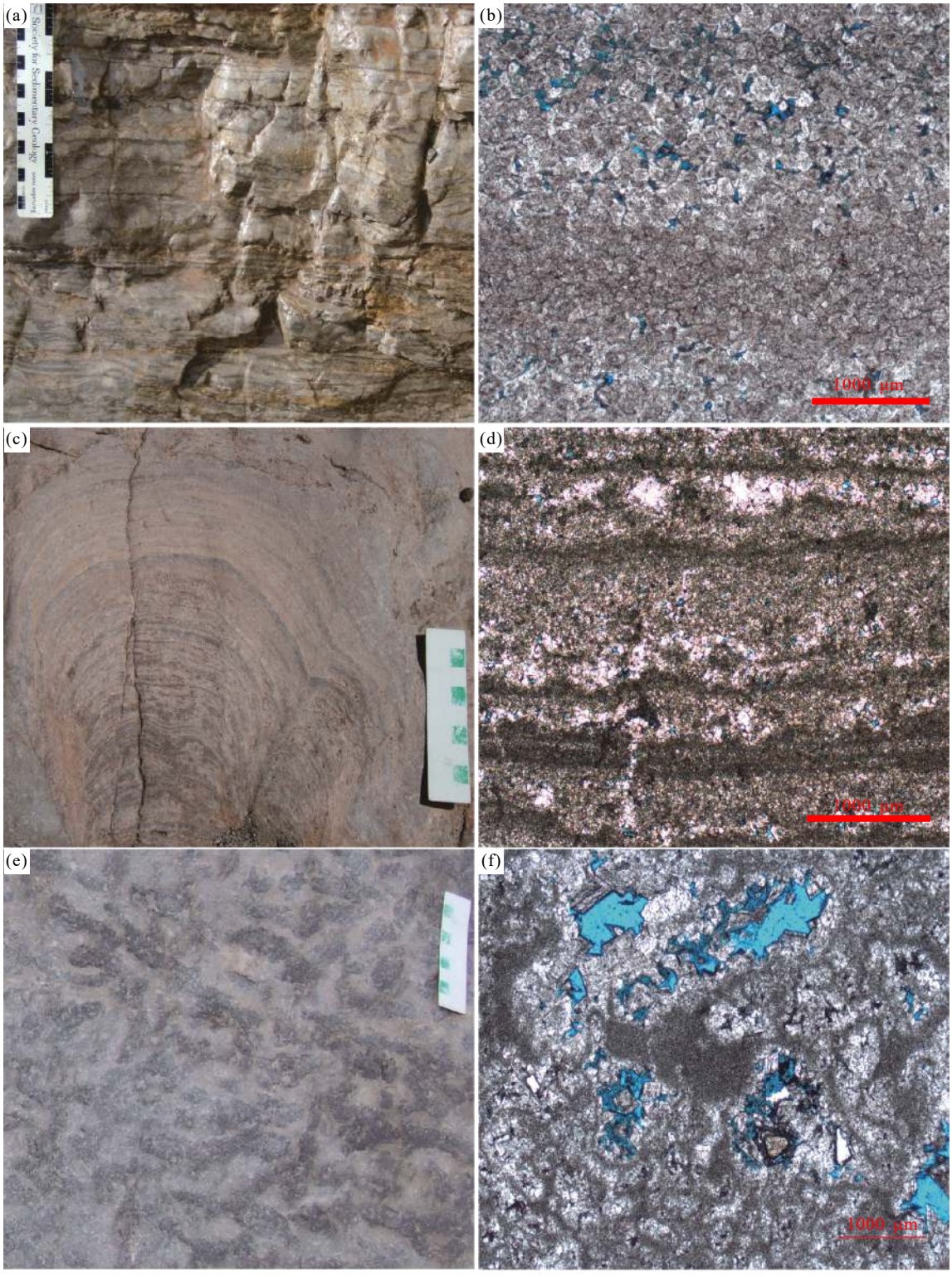

Fig. 4. Intertidal to restricted shallow subtidal facies. a–thick laminites (L2) with centimeter-scale laminae, TGL section. b–photomicrograph of thick laminites (L2) showing alternations of dark interlocking nonplanar dolomites and light finely planar dolomites. Abundant intercrystalline pores (in blue) are observed in PLB section. Planar-polarized light. c–domical stromatolite showing smooth to convoluted individual laminae (L4), PLB section. Scale in centimeters. d–photomicrograph showing stromatolite lamina with dark cryptmicrobial and light-colored, porous micropeloid couplets (pores are shown in blue), PLB section. Planar-polarized light. e–stratiform thrombolites (L5) with dendroid to digitate mesoclots, PLB section (Zhang YQ et al., 2015). Scale in centimeters. f–photomicrograph of thrombolite (L5) showing dark-gray irregular microbial micrite clots (or thromboses) and dissolution vugs (in blue), PLB section. Planar-polarized light. Blue areas are epoxy-impregnated porosity.

successions are dominated by shallow subtidal cycles with thin-bedded peloidal packstones/grainstones (L10) in base and thrombolite buildups (L9) or massive peloidal/ooidal grainstones (L8) in the cap (Fig. 9). The regressive

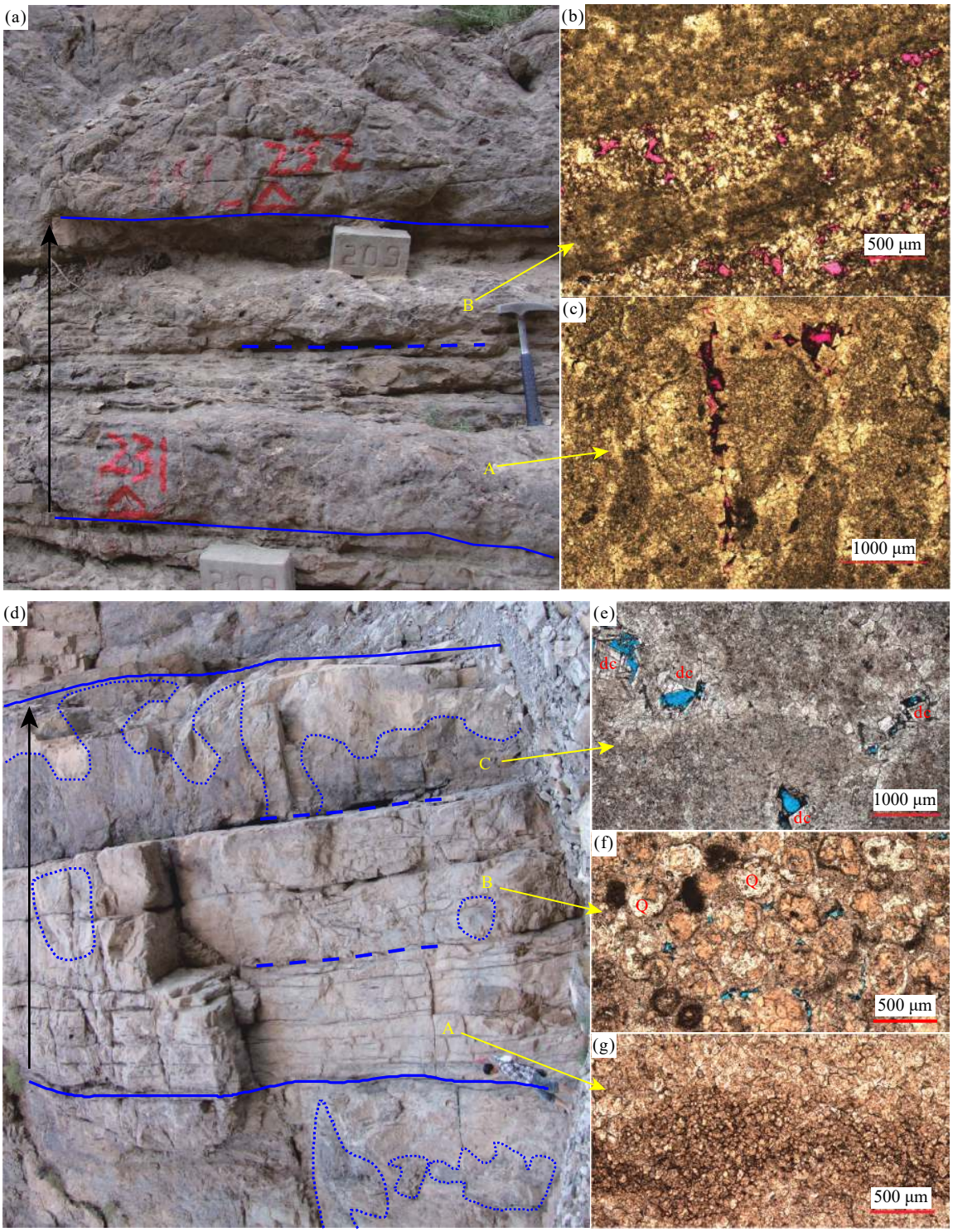

Fig. 5. Porosity distribution in cycles. a–peritidal cycle with a thrombolite base (A) and a stromatolite cap (B). Note the cap is more porous than the base of the cycle, PLB section. Hammer for scale (30 cm). b–photomicrograph of stromatolite (B in Fig. 5a). Note pores in red color. Planar-polarized light. c–photomicrograph of thrombolite (A in Fig. 5a). Note vugs in red color. Planar-polarized light. d–a typical shallow subtidal cycle with thin-bedded lenticular peloidal packstone/grainstone (L10, A) base, thick-bedded peloidal grainstone middle (B), and thrombolitic mounds (C, within dashed lines) cap, TGL section (Zhang YQ et al., 2015). Porosity increases upwards in a cycle. The standing person for scale (165 cm). e–photomicrograph of the thrombolite mound (C in Fig. 5d) showing small vugs (in blue) partly filled with planar dolomite cement (dc), TGL section. Planar-polarized light. f–photomicrograph of the thick ooidal grainstone (B in Fig. 5d) showing interparticle pores (in blue) and ghost ooids with quartz (Q) infills, TGL section. Planar-polarized light. g–photomicrograph of the thin peloidal grainstone (A in Fig. 5d) showing tightly compacted planar/nonplanar dolomite crystals with minor pores, TGL section. Planar-polarized light. Blue/red areas are epoxy-impregnated porosity.

successions are dominated by peritidal cycles with basal thick-bedded peloidal/ooidal grainstones (L8) grading upward to thin-bedded stromatolites/laminites (L4 to L1) caps (Zhang YQ et al., 2015).

5. Porosity variations in different facies

5.1. Porosity in intertidal to supratidal facies

The porosity and its distribution in each facies

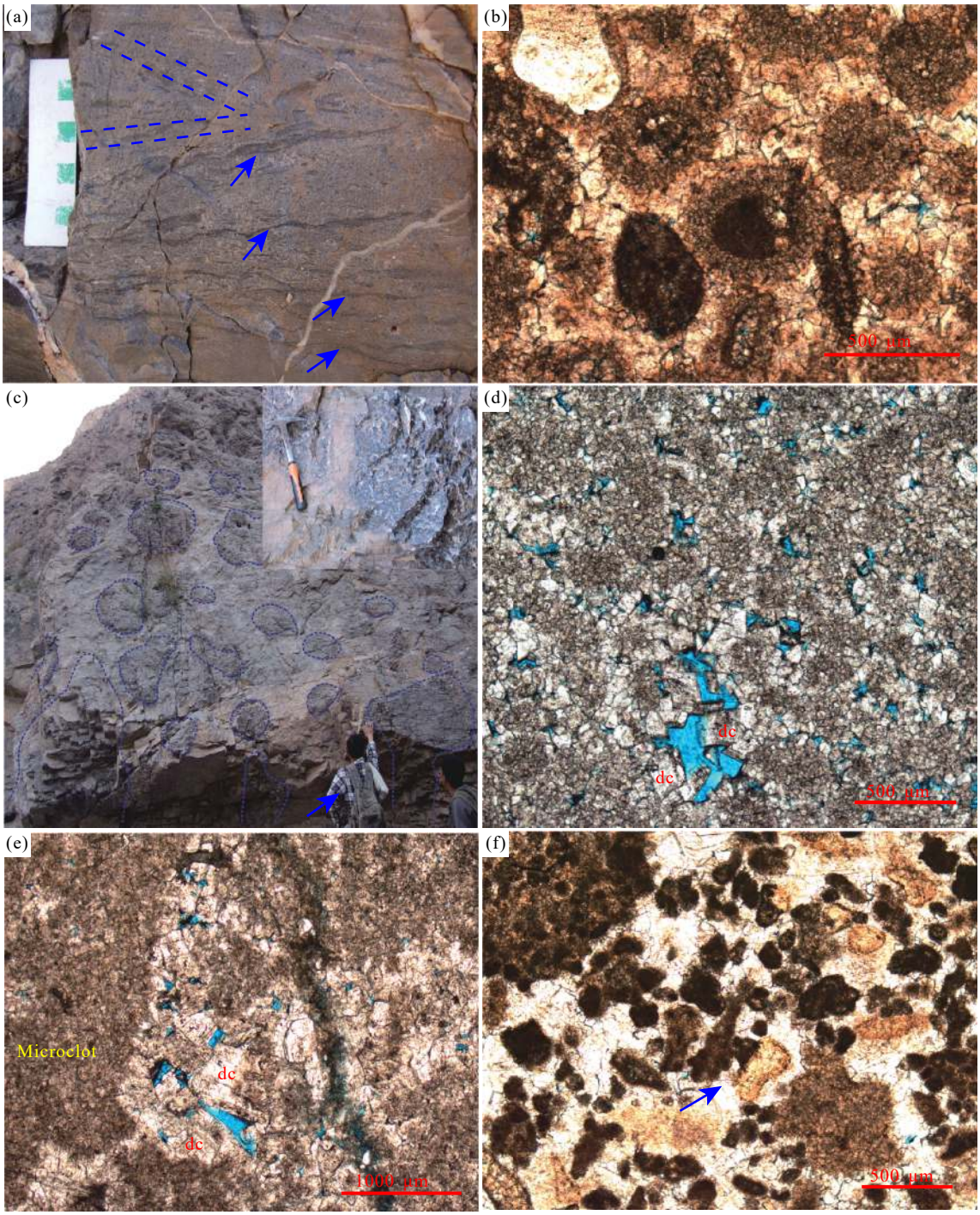

Fig. 6. Shallow subtidal facies. a–cross-bedded (dashed lines) pebbly peloidal-ooidal grainstone (L8) with multiple internal erosive surfaces (arrows), KP section(Zhang YQ et al., 2015). Scale in centimeters. b–pebbly peloidal-ooidal grainstone (L8). Note the vague internal fabrics of ooids are only with their ghosts and micrited peloids in pores (in blue), TGL section. Planar-polarized light. c–isolated, columnar microbial (thrombolite) buildups (L9, with circles) in the upper part of the Lower Qiulitag Group. Inter heads are filled with peloidal-ooidal grainstones (light-colored), TGL section. Standing person (left) for scale (about 0.7m). The inset photo shows the internal fabrics of the microbialite (Hammer is 30 cm). d–e– photomicrographs showing the microbial buildups (L9). Note vuggy and inter crystal porosity (in blue) and micro-clots (dark-brown color). Dolomite cement (dc) fills along pores, PLB section. Planar-polarized light. f–photomicrograph of peloidal grainstones (L11) showing micrited peloids mostly cemented by later dolomite crystals (white-gray color) and small pores (in blue). Note the presence of crinoid fragments (arrow). TGL section. Planar-polarized light.

associations were examined and presented in Table 2. The porosity is generally poor in thin laminites (0.1% to 8.5%; mean= 1.3%) and wavy laminites (0.1% to 4.0%; mean=1.9%). It is up to 8.5% in a few thin laminites (Table 2). The porosity in light-colored laminar within thick laminites (Figs. 4a, b) ranges from 1.0% to 12.5% (mean=4.7%). Notably, the high porosity in thick laminites is mostly present in the caps of cycles. The porosity in L1, L2, and L3 is dominated by intercrystal pores with minor vugs. Most pores are partly filled by calcite crystals and later dolomite.

Stromatolites (L4; Figs. 4c, d) are composed of intergrown microbial or cryptmicrobial laminae. The porosity is abundant in stromatolites, ranging from 0.1% to 12.5% (mean=6.0%), commonly between 3.0% and 10.0% (Tables 1, 2). The stromatolites with high porosity are mainly present in the lower-middle parts of cycles. The stromatolites are dominated by fenestral and intercrystal pores (Fig. 4d) with few interpartical pores and vugs. Most pores are partly filled with quartz, coarse dolomite crystals, and organic materials within L4.

5.2. Porosity in restricted shallow subtidal to lower intertidal facies

In thrombolites, the porosity (L5) ranges from 0.1% to 15.0% with a mean value of 4.9% (Table 2), which is dominated by intercrystal and vuggy pores (Figs. 4f, 5c). Abundant inter-clot pores or cavities are filled by fibrous to blade sparry carbonates (calcite) and/or internal silt-sized sediments (Figs. 4e, f). Besides, few dissolution pores are present in some calcite crystals, indicating later corrosion. In pisolitic grainstone (L6), the porosity is abundant with a range from 1.8% to 16.5% (mean=7.5%), which is dominated by intercrystal and interpartical pores with minor intrapartical pores. Notably, the bitumens are present in some pores of L6. In ribbon mudstone to packstone (L7), the porosity is less common with a range from 0.1% to 8.2% (mean=2.7%; Table 2), which is mainly characterized by intercrystal and vuggy pores with few intrapartical pores. Some bitumens and quartzs are observed in pores of L7.

5.3. Porosity in open-marine subtidal facies

In oolite (L8), the porosity ranges from 0.2% to 20.0% (mean=3.1%), while mostly from 1.0% and 3.0% (Table 2). High porosity (>4.0%) is locally present in the upper part of the Lower Qiulitag Group in many sections. Oolite is dominated by intercrystal and vuggy pores with minor interparticle, intrapartical, moldic pores (Figs. 5f, 6b) and fractures. Most pores within L8 are partly filled by coarser dolomite, calcite, quartz, and bitumen. In microbial buildups (L9), the porosity ranges from 2.0% to 25.0% (mean=6.9%), commonly between 3.0% and 3.9% (Table 2). The porosity is generally intercrystal and vuggy pores (Figs. 5e, 6d, e) with minor channel and fracture in L9. The pores within L9 are

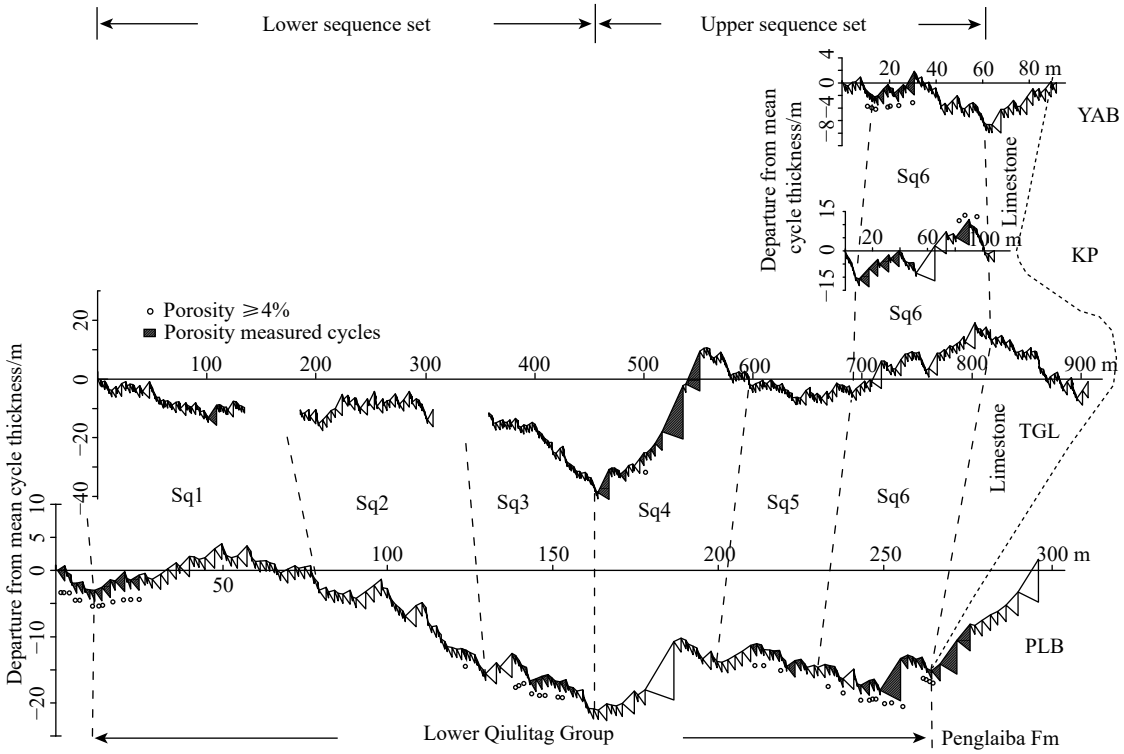

Fig. 7. Porosity distribution in meter-scale cycles and sequences of the Lower Qiulitag Group from the four measured sections (see Fig. 1 for the location; modified from Zhang YQ et al., 2015). Sequence stacking patterns reveal a synoptic accommodation (or sea-level) decrease from Sq1 to Sq3 and an increase from Sq4 to Sq6, defining two sequence sets. Abundant porosity is generally present in peritidal cycles of regressive successions and in thick shallow subtidal cycles of transgressive successions. Porosity-measured cycles are marked by shade. Porosity ⩾4% is marked on the side of cycle curves.

partly filled by later dolomite, calcite, quartz, and bitumen. In lenticular to platy dolomite (L10), the porosity commonly developed in the upper part of the Lower Qiulitag Group in multiple sections, ranging from 0.1% to 10.0% (mean=3.4%). It is dominated by intercrystal and vuggy pores with minor small moldic pore and fracture. Most pores within L10 were occluded by later coarse dolomite and quartz crystals.

6. Porosity variations and stratal cyclicity

6.1. Porosity in meter-scale cycles

Hundreds of shallowing-upward, meter-scale cycles are developed in the Lower Qiulitag Group, ranging from 0.3 m to 18 m (average 2.3 m) in thickness. The porosity is variable in different types of cycles. In the thrombolite-based peritidal cycles, the porosity shows two trends from base to top of cycles, as their difference in caps. In the thrombolite-stromatolite-thick/wavy laminite cycles, the porosity generally shows an increasing trend from base to top of cycles (Figs. 3, 5a–c). Based on the data collected, the porosity is about 2.0%–8.3% in the basal thrombolites, 3.0%–12.5% in the middle stromatolites, and 8.5% –16.5% in the upper thick/wavy laminites (Fig. 8). The presence of abundant pores in laminites was probably derived from freshwater dissolution, as evidenced by the occurrences of vug (Moore CH, 1989; Tucker ME, 1993). While in the thrombolite-stromatolite-thin laminite cycles, the porosity increases from thrombolite (2.0%–8.3%) to stromatolite (3.0%–12.5%), and decreases in the thin laminite-cap (0.1%–0.4%; Fig. 8).

As described above, there are two subtypes of shallow subtidal cycles. The distribution of porosity is different in these two subtype cycles. In the cycle with basal lenticular-platy peloidal wackestones/packstones (L10) and thick-bedded peloidal-ooidal grainstones cap (L8; Fig. 3B), the porosity is low in bases while high in caps, displaying an increasing trend upwards within individual cycles. In the cycle with a similar basal lithofacies (L10) capped by microbial buildups (L9; Figs. 3A, 5d), the porosity is high in the basal lithofacies while low in the cap, showing a decreasing trend upwards within individual cycles. However, in most shallow subtidal cycles, the grainy upper parts are

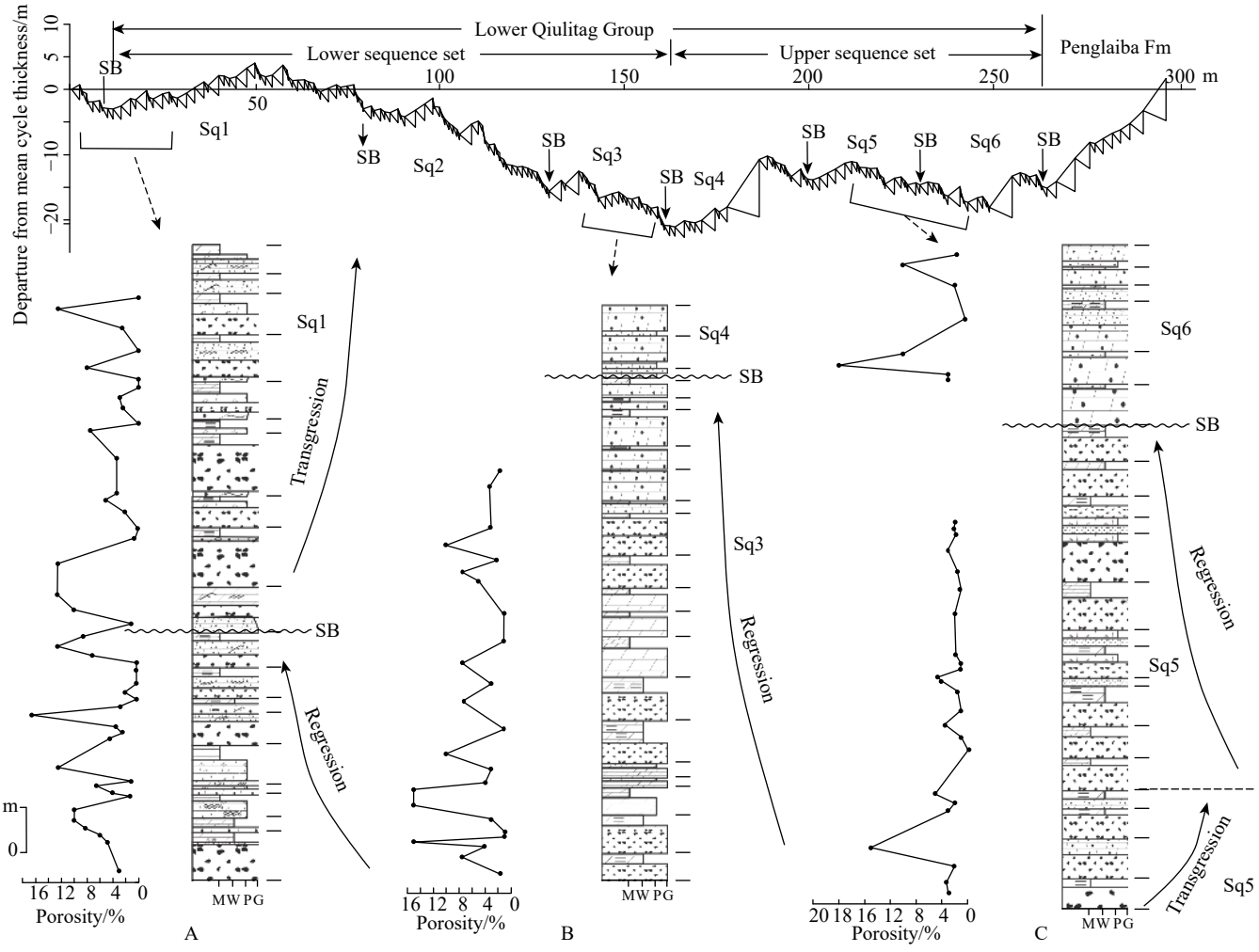

Fig. 8. Porosity distributions in the third-order transgressive-regressive succesions of the Lower Qiulitag Group at the PLB section. High porosity is widely present in the thick thrombolites and thick-laminites in the transgressive intervals. The porosity increases upwards in cycles in the lower part, while decreases upwards in cycles in the upper part of the regressive succession of Sq3. Abundant porosity occurs around sequence boundaries. SB−Sequence boundary. Short lines on the right of logs mark the cycle boundaries. See Fig. 3 for the legend.

commonly subjected to more or less dolomitization, silicification, and recrystallization, resulting in fabric (or structures) destruction or obliteration, and porosity decrease (Fig. 5f; see following discussions).

6.2. Porosity in third-order sequences

Six third-order depositional sequences (Sq1 to Sq6) are grouped into larger-scale sequence sets: The lower (Sq1 to Sq3) and the upper (Sq4 to Sq6; Figs. 7, 8). In the lower sequence set (Sq1 to Sq3), peritidal facies overwhelmingly predominate even in the lower part of the sequences. Based on the measured data, relative high porosity occurs in the lower transgressive part, especially in some lower-middle parts of cycles (Fig. 8), reflecting a facies-selective character of porosity development. The porosity shows a decreasing-upward trend from the lower to the middle transgressive part (Fig. 8; Sq1). Notably, in Sq3, the porosity increases upwards within individual cycles in the early regression, while the porosity subsequently decreases upwards in upper cycles in the late regression.

In the upper sequence set (Sq4 to Sq6), sequences are dominated by shallow subtidal facies (i.e., L8 and L9; Fig. 9), even in the upper parts (regressive intervals) of some sequences (i.e. at KP section). In general, the porosity is low in shallow subtidal cycles of the transgressive successions, although high porosity is locally present. The porosity commonly shows a decreasing trend from the lower cycles to the upper cycles in the transgressive intervals, while an increasing trend in the regressive intervals.

Additionally, a large variety of porosity occurs around sequence boundaries (Fig. 9), i.e. ranging from 0.8% to 6.0% between Sq5 and Sq6 at the YAB section (Fig. 9C). In general, the abundant porosity is well present in 1–4 m depths below the sequence boundary (subaerial exposure surface) (Figs. 8, 9). Beneath sequence boundaries, vugs in peloidal/ooidal grainstones (L8) are largely present and partly filled with later dolomites and calcites (Fig. 10).

7. Controls on porosity development and preservation

The development of porosity in carbonates is quite complex, which is generally influenced by primary sedimentation and late diagenetic processes (Moore CH,

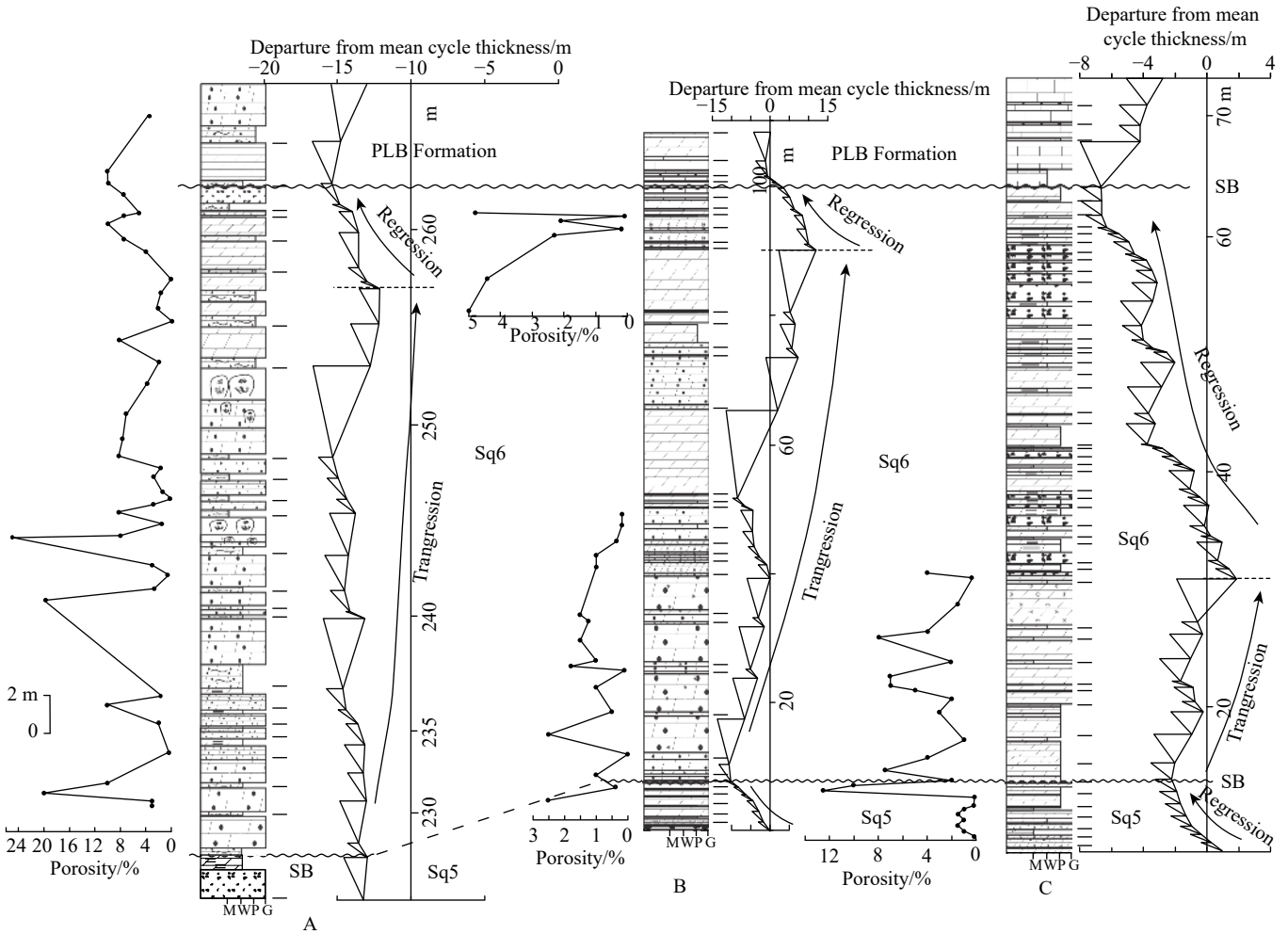

Fig. 9. Porosity distribution in the third-order sequence Sq6 of the Lower Qiulitag Group. Abundant porosity generally occurs in the thick subtidal cycles during the transgressive stage. The porosity commonly shows an upward-decreasing trend in the transgressive intervals. The porosity is extremely variable around sequence boundaries (between Sq5 and Sq6). A–PLB section; B–KP section; C–YAB section. SB−Sequence boundary. Short lines on the right of logs mark the cycle boundaries. See Fig. 3 for the legend.

1989; Tucker ME, 1993; Saller AH et al., 1994; Moore CH and Wade WJ, 2013). It 's well known that late diagenetic processes, such as compaction, recrystallization, calcitization, and silicification, tend to reduce the host rock porosity; while

Table 2. Measured porosity (%) in lithofacies of the Lower Qiulitag Group in the study area.

Thin laminite (L1)	Sample	Thick laminite (L2)	Sample	Wavy laminate (L3)	Sample	Stromatolite (L4)	Sample	Stratiform thrombolite (L5)	Sample	Stratiform thrombolite (L5)	Sample
6	PL-275	6.8	PLW-23	2.1	PLW-22	10.1	PLW-9	3.1	PL-273	10	PL-443
1.25	PL-277	8.1	PLW-30	0.1	TG-41	6.5	PL-279	4	PL-283	7.5	PL-445
0.2	PL-288	10	PLW-32	1.5	TG-43	12.5	PL-281	3.5	PL-285	7.5	PL-447
0.2	PL-292	7.5	PL-430	1	TG-102	5	PL-304	2	PL-289	5	PL-451
8.5	PL-295	1	PL-433	2.5	SN-02	7.5	PL-307	7	PL-293	7.5	PL-452
0.1	PL-302	3	PL-436	4	YAB-25	3	PL-311	10	PL-298	10	PL-454
0.1	PL-308	15	PL-439			12.5	PL-317	12.5	PL-300	3	PLW-37
0.1	PL-312	1	PL-444			7.1	PL-358	2	PL-303	0.1	PL-483
0.1	PL-313	3	PL-446			11	PL-398	3.4	PLW-12	1	PL-484
0.1	PL-318	3.3	PLW-38			1	PL-489	2.5	PL-310	1	PL-486
1	PL-448	3	PL-480			1.7	PLW-42	8	PL-314	4	PL-488
1	PL-450	5	PL-482			0.1	TG-38	2.5	PL-316	1	PL-491
2	PL-453	3.5	PL-485			0.4	SN-03	3.4	PL-357	2	PL-492
3	PL-455	1.5	PL-487					2.4	PL-368	1.5	PL-494
0.1	TG-44	1.8	PL-490					4.3	PL-389	2.9	PLW-40
0.1	TG-82	1	PL-493					5.8	PL-391	10	PL-532
0.1	SN-39	2	PL-501					2.6	PL-396	7.5	PL-537
0.2	SN-40	2	TG-85					6.3	PLW-31a	10	PL-539
1	YAB-14	12.5	YAB-20					1.5	PL-429	3.6	PL-571
1	YAB-16	2	YAB-23					4	PL-431	1	TG-81
1	YAB-17							15	PL-432	0.1	TG-88
0.1	YAB-19							1	PL-434	1.25	TG-103
2	YAB-32							15	PL-438	4	YAB-37
Cross-bedded Gs lentil (L6)	Sample	Thin-bedded ribbon dolomite (L7)	Sample	Oolite (L8)	Sample	Oolite (L8)	Sample	Microbial buildups (L9)	Sample	Lenticular to platy dolomite (L10)	Sample
4.9	PL-274	8.2	Pl-276	2	PL-481	1	SN-04	2	PL-478	3	PL-442
2.5	PL-284	4	PL-278	20	PLW-45	0.1	SN-06	25	PL-509	3.1	PLW-44
16.5	PL-286	1	PL-280	0.4	PL-500	0.1	SN-07	8	PL-511	5	PLW-46
1.8	PL-290	3	PL-287	10	PL-502	2.5	SN-08	7.5	Pl-521	1.5	PL-503
12.5	PL-294	0.2	PL-292	20	PL-505	1	SN-10	3.9	Pl-522	3	PL-506
1	PL-297	3.4	PL-305	0.4	PL-507	0.1	SN-12	3.5	PL-546	2.5	Pl-517
12.5	PL-299	0.1	PL-313	3	PL-508	1.8	SN-14	3	TG-95	2.2	Pl-523
0.4	PL-301	2.2	PL-367	1.5	Pl-512	1	SN-16	3	TG-96	0.1	Pl-525
15	PL-479	3.3	PL-456	3	Pl-514	1.5	SN-17	3	TG-97	1.7	Pl-527
		1.7	PL-457	3	PL-497	1.25	SN-18	10	YAB-21	7.5	PL-531
				1.5	Pl-516	1.5	SN-19			7.5	PL-533
				1.8	Pl-518	1	SN-21			10	PL-538
				8	Pl-520	1	SN-23			1.5	TG-83
				8.5	Pl-524	0.4	SN-24			0.1	TG-86
				2.4	Pl-526	0.2	SN-26			0.1	TG-87
				4	PL-530	2	SN-33			0.1	TG-88
				5	PL-534	4.4	SN-36			0.4	TG-89
				5	PLW-52a	2.3	SN-37			1	TG-83
				2	PL-572	2.1	KPM-5			5	TG-94
				1.5	TG-36	4.8	KPM-18			5	YAB-29
				2.5	TG-37	0.2	YAB-13			7	YAB-30
				2.5	TG-39	1.5	YAB-15			2	YAB-32
				5	TG-42	7	YAB-30			8	YAB-33
				0.1	TG-84	4	YAB-33				
				1	TG-83	1.5	YAB-35				
				1	TG-100						

corrosions and fracturing tend to enhance porosity of the host rocks (Hu MY, 1993; Zheng HR et al., 2007; Huang WH et al., 2012; Hu MY et al., 2019). In this study, a few pore spaces are partially filled by later quartz and calcite crystals, reducing the porosity of dolomites. Notably, late-stage calcite cements are the most common fillings postdating all types of dolomite. On the other hand, the small moldic pores and fractures are locally present in the Lower Qiulitag Group, indicating various corrosions associated with organic or sulfuric acids and fracturing could have created/enlarged pores during later diagenetic processes (Mazzullo S and Harris P, 1992; Ye DS, 1994; Cai C et al., 2001; Ngia NR et al., 2019). Thus, late diagenetic processes should have played roles in the development of porosity in the Lower Qiulitag Group. However, diagenetic modifications on porosity, such as recrystallization, calcitization, dolomitization, and silicification may more or less inherit from primary sedimentary compositions and fabrics (Moore CH, 1989; Tucker ME, 1993; Lucia F and Major R, 1994; Sun SQ, 1995; Saller AH et al., 2001). Furthermore, spaces or pathways for later fluids circulation and precipitation during deep burial stages may benefit from primary porosity distribution that derive from the different scales of cyclic framework and duration of subaerial exposures (James NP and Choquette PW, 1988; Loucks RG and Sarg JF, 1993; Fan TL et al., 2007; Yu BS et al., 2007; Liu JD et al., 2009). Importantly, the significantly heterogeneous distributions of porosity in facies, individual cycle, and third-order sequence in the Upper Cambrian Lower Qiulitag Group definitely support a differential controlling on porosity development, which is most likely by the variable scales of sea-level fluctuations. Thus, the relationships of porosity distribution with facies and cyclicity, and related controlling factors (especially sea-level fluctuation) are further been discussed.

7.1. Facies controls

The distribution of porosity is featured with facies selective in this study. The relative high porosity is present in thick laminite (L2), stromatolite (L4), thrombolite (L5), cross-bedded packestone/grainstone lentil (L6) and microbial buildup (L9), while the low porosity is present in thin laminite (L1), wavy laminite (L3), thin-bedded ribbon mudstone to packstone (L7; Fig. 11; Table 2). The low porosity in those lithofacies is associated with their lower energy conditions of shallowing-upward tidal flats, such as laminites (Lindsay RF and Kendall CGSC, 1985; Tucker ME et al., 1990). While the relatively high porosity in those lithofacies is associated with their primary grain-rich and/or frame-building organism facies types (Fig. 3), such as L4, L5, L6, and L9. All these features suggest that the porosity development is controlled by primary depositional environments (Tucker ME et al., 1990; Moore CH, 2001).

7.2. Stratal hierarchical controls

The sedimentary cyclicity plays a major role in porosity distribution in host rocks (Stemmerik L and Larssen GB, 1993; Saller AH et al., 1994; Eichenseer HT et al., 1999; Saller AH et al., 1999a; Moore CH, 2001). As described above, pore-rich lithofacies are widely present in the lower-middle parts of cycles which are commonly capped by thin laminites (L1; Figs. 8, 9). In this case, these tight caps (such as thin laminites) would have prevented the later diagenetic fluids circulating in the caps and also the basal lithofacies of cycles (e.g. Moore CH, 2001), enhancing pores preservation in the lower lithofacies (such as thrombolites and stromatolites) of cycles. In contrast, due to the absence of laminitis-caps in some cycles, later diagenetic fluids might have readily penetrated primary pores, leading to later dolomite or calcite precipitations and fillings. Thus, many ooidal grainstones (L8) or microbial buildups (L9) of shallow subtidal cycles display relatively low porosity in the study area, which are probably resulted from strong modification (e.g. dolomitization and/or recrystallization) during the late diagenetic stage.

In addition, many previous studies have suggested that the duration of subaerial exposure in response to variable scales of sea-level change has a significant impact on the porosity development in carbonates (James NP and Choquette PW, 1984; Esteban M and Wilson JL, 1993; Saller AH et al., 1994, 1999a). The porosity of cyclic carbonate could be increased by meteoric dissolution or decreased by sub-seafloor authigenic minerals (i.e. calcite and dolomite) precipitation, which is closely related to the duration of subaerial exposure. In general, a moderate duration of subaerial exposures could lead to relatively higher porosity by meteoric dissolution (Stemmerik L and Larssen GB, 1993; Saller AH et al., 1994; Eichenseer HT et al., 1999; Saller AH et al., 1999a). On the other hand, the prolonged subaerial exposure sustaining relatively stable diagenetic zonation could reduce carbonate porosity due to persistent mineral (such as calcite and dolomite) precipitations in each favorable zone. In this study, each of the cycles is terminated by an event of subaerial exposure related to high-frequency sea-level falling (Zhang YQ et al., 2015). Porosity generally increases upward within individual cycles (Figs. 5a, 8), especially in a few thrombolites (L5)-stromatolite (L4)-laminite (L2/L3) of peritidal cycles (Fig. 5a –c) and in peloidal wackestones/packstones (L10)-grainstones (L8) of shallow subtidal cycles. Abundant pores in the top of cycles might be favored by meteoric leaching during brief to moderate subaerial exposures (Stemmerik L and Larssen GB, 1993; Saller AH et al., 1994; Eichenseer HT et al., 1999; Saller AH et al., 1999a). This suggestion is also consistent with the results from the wells in NW Tarim Basin, where the porosity in the tops is higher than that in the bases of cycles in deeply burial environment (Yu BS et al., 2007; Liu JD et al., 2009; Zhao WZ et al., 2014). However, a decreasing trend of the porosity from the base to the top of cycles is also present in certain cycles (Figs. 8, 9), such as in peritidal cycles capped by thin laminites/tight mudstones and in shallow subtidal cycles capped by microbial buildups/ooidal grainstones (Fig. 3). This

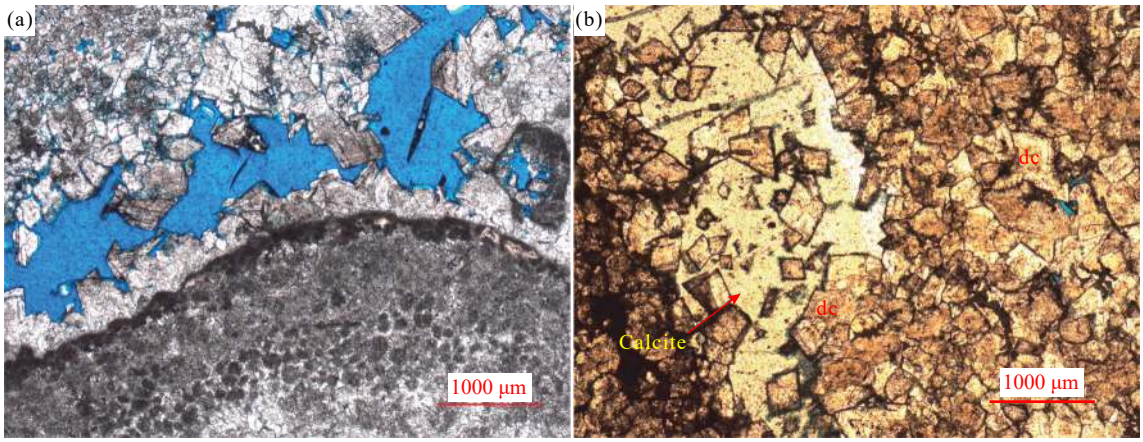

Fig. 10. Photomicrographs showing vuggy pore in grainstones below the sequence boundaries. Planar-polarized light. a–vugs (in blue) in the peloidal-ooidal grainstones. Note vugs are largly unfilled. PLB section. b–vugs in planar matrix dolomites. Note vugs are filled by large calcite crystal and dolomite cements (dc). Floating planar dolomites are present on the surfaces of calcite crystals, KP section.

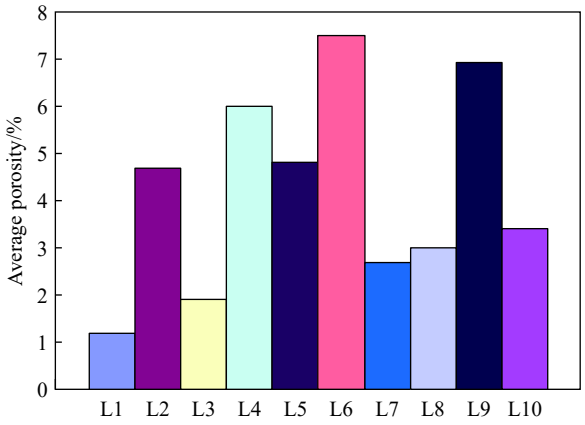

Fig. 11. The distribution of porosity in lithofacies of the Lower Qiulitag Group. The high porosities (>4.0%) are present in L2, L4, L5, L6 and L9.

scenario may be caused by variable factors. Generally, thin laminites/mudstones caps deposited in lower energy conditions of shallowing-upward tidal flats, which may be favorable for tight accumulation and low porosity (Lindsay RF and Kendall CGSC, 1985; Tucker ME et al., 1990). In contrast, microbial buildups/grainstones caps of cycles have suffered later intensive dolomitization, also leading to low porosity (see the following discussion; Fig. 9). Furthermore, the caps of cycles may be significantly influenced by very brief, which may be the additional factor contributing to low porosity (Saller AH et al., 1999a). Consequently, the top part bears relatively low porosity with respect to the basal part in some cycles.

On a large scale, the third-order sea-level fluctuation plays an important role in the development of carbonate porosity in the studied intervals. The distribution of porosity is highly variable in the transgressive and regressive successions of six third-order sequences. The previous study suggested that the exposure diagenesis with pore generations was dominated during the early transgressive stage, while the marine diagenesis with the reduction of porosity was dominated in the later transgressive stage (e.g. Moore CH, 2001). This scenario is also evidenced in this study that the porosity is relatively higher in the cycles of the lower transgressive parts than that in the upper transgressive parts within the sequences (Fig.9). However, the distribution of porosity in the regressive successions is quite complex (Figs. 8, 9). In the lower sequence set (Sq1 to Sq3), the porosity is relatively abundant in the peritidal cycles of the regressive successions, which may derive dominantly from exposure-related diagenesis (Moore CH, 2001). On the other hand, the porosity is less abundant in the thick cycles of the transgressive successions, since marine diagenesis is dominant during the longer-term sea level falling. Additionally, the porosity, showing an upward-decreasing trend, is quite low at the end of Sq3. This scenario could be reasonably interpreted as a result of prolonged subaerial exposure related to a higher, long-term (likely as second-order) sea-level fall (Fig. 8B), which have increased calcite precipitation in primary pores (Saller AH et al., 1999a). In the upper sequence set (Sq4 to Sq6), however, in some cases, the porosity is less abundant in the thinner cycles of the regressive successions, such as tightly compacted dolomites in thick-bedded peloidal/ooidal grainstones (L8). This scenario may result from a short period of subaerial exposure, which is unable to create abundant pores by freshwater dissolution in the background of long-term sea-level rise (Saller AH et al., 1999a).

Although sequence boundaries are characterized by generally gradational and conformable stratigraphic intervals in the Lower Qiulitag Group (Figs. 8, 9, 10), the porosity is highly variable among them. Abundant porosity (about 12.5%) is present in the intervals at shallow depth (about 1–4 m) below the sequence boundary (subaerial exposure surface; Figs. 8A, 9), where residual vugs with minor calcite cement are preserved in dolomite matrix within grainstones (Fig. 10a). This scenario could be reasonably interpreted as that the period of subaerial exposure is favorable to generate pores by dissolution and to confine the calcite precipitations (Stemmerik L and Larssen GB, 1993; Saller AH et al., 1994; Eichenseer HT et al., 1999; Saller AH et al., 1999a). In contrast, the intervals at a shallower depth (<1 m)

immediately below the subaerial exposure surface contain relatively poor pores, as vugs being largely filled by coarse dolomite, quartz or calcite cement in some ooidal grainstones (L8; Fig. 10b). This scenario may be caused by prolonged subaerial exposure (Saller AH et al., 1999a). Consequently, the porosity distribution around sequence boundaries in the Lower Qiulitag Group is closely related with the duration of subaerial exposures (Saller AH et al., 1994; Dickson J and Saller AH, 1995; Saller AH et al., 1999a; Carlson RC et al., 2003).

7.3. Diagenetic controls

The Lower Qiulitag Group in the study area is completely dolomitized. Six types of matrix dolomite are identified, including micrite, relict mimetic, floating planar, fine-coarse planar, fine-coarse nonplanar, and saddle dolomite (Fig. 12; Sibley DF and Gregg JM, 1987; Dong SF et al., 2017). Two kinds of dolomite cement are present, namely planar dolomite cement and saddle dolomite cement (Figs. 6d –e, 12e –f). These different dolomite types are a result of complex and multiphase dolomitizations, such as biologically mediated precipitation during contemporaneous stage (You X et al., 2013), seepage-reflux during penecontemporaneous to the early diagenetic stage (Ye DS, 1992; Shao LW et al., 2002; Shen AJ et al., 2009; Huang WH et al., 2012; Zheng JF et al., 2012; Chen YQ et al., 2013; Wang XL et al., 2018), and hydrothermal alteration during deep burial stage (Dong SF et al., 2013; Zhu DY et al., 2015). Notably, matrix and cement dolomite both are mainly controlled by depositional facies. For example, micritic dolomites in this study area are generally associated with laminites in the interior platform, lagoon, and tidal flat, being subject to complete dolomitization. Relict mimetic dolomites mainly developed in peloidal/ooidal grainstones (L8) and/or organic framework dolomites (e.g. thrombolite). They commonly occur in reef and shoals near the platform margin, in the microbial buildups of the interior platform, and/or in grainstones of the tidal channel. The planar dolomites developed in grainstones/packstone, particularly in the upper part of the Lower Qiulitag Group.

In general, the effect of dolomitization on porosity is variable (Choquette PW et al., 1992; Lucia F and Major R, 1994; Purser B et al., 1994), especially in different types of dolomite in Tarim Basin (Hu MY, 1993; Ye DS, 1994; Shen AJ et al., 2009; Huang WH et al., 2012; Zhao WZ et al., 2014; Zhu DY et al., 2015; Hu MY et al., 2019). Porosity in dolomites is inherited mostly from precursor carbonates (Purser B et al., 1994; Zhao WZ et al., 2014). In this study, the porosity is relatively high in most thrombolites (L5) and microbial boundstones (L9) developed near the platform margin. This may result from that dolomitizing brines in this region are not sufficient to induce complete dolomitization (Saller AH and Henderson N, 1998), leaving some pores unfilled. The intercrystal pore is common in the planar dolomite matrix (Figs. 4b, 12c). In contrast, the vuggy pore is common in all types of dolomite (Figs. 4–6, 10, 12), as a result of different stages of dissolution related to variable scales of sea-level fall (Fan TL et al., 2007; Yu BS et al., 2007). Because potential modifications on porosity distribution by multistage dolomitization have been extensively investigated in Cambrian dolomites in Tarim Basin, and it has been suggested that the well-developed porosity of Upper Cambrian dolomites in deep subsurface was significantly related with burial and hydrothermal dolomitization (Zhao WZ et al., 2014; Zhu DY et al., 2015). It is, therefore, not the authors' interest to discuss them in detail in this paper.

8. Porosity evolution in the cyclic stratigraphic framework

The cyclic dolomites in the Upper Cambrian Lower Qiulitag Group in the study area are formed in response to variable sea-level fluctuations (Zhang YQ et al., 2015). The distribution of porosity is highly heterogeneous in the Lower Qiulitag Group, which is controlled by many factors. Firstly, the porosity distribution is facies-selective, with the evidence of high porosities widely presenting in primary grain-rich and/or frame-building organism facies types, such as thick laminite, stromatolite, thrombolite, cross-bedded packestone/grainstone, and microbial buildup. This scenario is consistent with the suggestion that porosity development derives from primary sedimentation (Tucker ME et al., 1990; Moore CH, 2001). Secondly, the porosity distribution is in response to the sedimentary cyclicity associated with different scales of sea-level fluctuations (Goldhammer R et al., 1990; Read J and Horbury AD, 1993; Saller AH et al., 1999b; Moore CH, 2001), with the evidence of pore-rich lithofacies commonly presenting in the lower-middle parts of cycles which are commonly capped by thin laminites (L1; Figs. 8, 9). Thirdly, the development and distribution of porosity are causally linked to the duration of subaerial exposure (around cycles and sequences) associated with different sea-level fluctuations (James NP and Choquette PW, 1984; Esteban M and Wilson JL, 1993; Saller AH et al., 1994, 1999a). It is generally believed that very brief or no subaerial exposure could result in rare pores, while the brief to moderate subaerial exposures could lead to relatively higher porosity by meteoric dissolution, whereas the prolonged subaerial exposure could reduce porosity due to more calcite precipitations. Moreover, other diagenetic modifications (such as dolomitization, compaction, corrosions, fracturing, recrystallization, calcitization, and silicification) on porosity are inherited from primary sedimentary compositions and fabrics (Moore CH, 1989; Tucker ME, 1993; Lucia F and Major R, 1994; Sun SQ, 1995; Saller AH et al., 2001), which are further controlled by different scales of cyclic framework and duration of subaerial exposures (James NP and Choquette PW, 1988; Loucks RG and Sarg JF, 1993; Fan TL et al., 2007; Yu BS et al., 2007; Liu JD et al., 2009). Therefore, the porosity distribution in the Lower Qiulitag Group is overwhelmingly controlled by the depositional facies and cyclicity (characters of cycles,

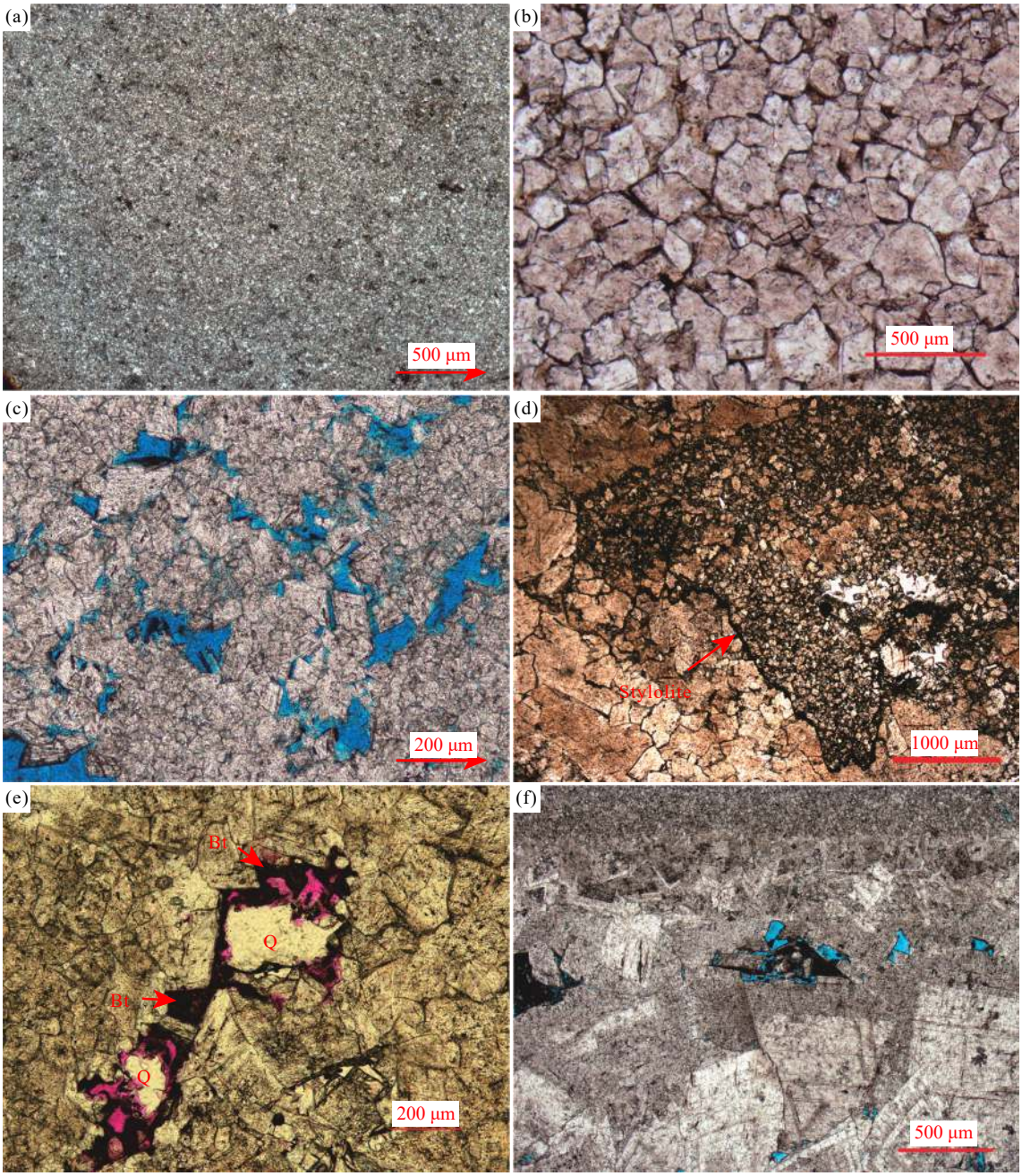

Fig. 12. Photomicrographs of dolomite types and related porosity. Planar-polarized light. a–micritic dolomite, PLB section. b–planar dolomite, TGL section. c–planar dolomite with vuggy and intercrystalline porosity (in blue), PLB section. d–planar and nonplanar dolomites separated by stylolite, KP section. e–the vug (in red) partly filled with bitumen (Bt) and quartz (Q), PLB section. f–saddle dolomites showing curved crystal face along the pores. Small pores are preserved in the center of pore spaces (in blue), KP section.

sequences) related to different scales of sea-level fluctuations.

9. Conclusion

Porosity distributions in the Upper Cambrian Lower Qiulitag Group dolomites in northwestern Tarim Basin are highly heterogeneous in individual facies, cycles, and sequences. Thick laminite (L2), stromatolite (L4), thrombolite (L5), cross-bedded packestone/grainstone lentil (L6), and microbial buildup (L9) generally bear abundant porosity, indicating a facies-selective feature. Furthermore, porosity distributions are closely dependent on meter-scale cycle patterns and third-order transgressive-regressive sequence framework. The relatively high porosity is present in the microbialite-based peritidal cycles and thin cycles (peritidal cycles dominated) of regressive successions. The abundant porosity generally occurs below the third-order sequence boundaries. Thus, porosity development and preservation in the Lower Qiulitag Group thick dolomite successions are primarily controlled by facies which were influenced by sea-level fluctuations of different orders and later diagenetic overprinting. The findings in this study are expected to be helpful in better understanding the porosity distribution in cyclic dolomites, which may provide implications for future

hydrocarbon exploration in Tarim Basin and elsewhere.

CRediT authorship contribution statement

Yan-qiu Zhang and Dai-zhao Chen conceived of the presented idea. Yan-qiu Zhang developed the theory, performed the computations and verified the analytical methods. Dai-zhao Chen supervised the findings of this work. All authors discussed the results and contributed to the final manuscript.

Declaration of competing interest

The authors declare no conflict of interest.

Acknowledgment

This study was funded by geological survey projects of China Geological Survey (DD20190405, DD20190406), National Science and Technology Special Project of China (2011ZX0500803) and National Basic Research Project (2012CB214802). Yan-qiu Zhang thanks the student scholarships from University of Potsdam.

References

Cai C, Hu W, Worden RH. 2001. Thermochemical sulphate reduction in Cambro –Ordovician carbonates in Central Tarim. Marine and Petroleum Geology, 18, 729–741. doi: 10.1016/S0264-8172(01)00028-9.

Cai XY, Mao SH, Qian YX. 2009. Stratigraphic classification and correlation of Cambrian in Bachu uplift, Tarim basin Xinjiang. Petroleum Geology, 30, 38–42 (in Chinese with English abstract). doi: 10.1016/S1874-8651(10)60080-4.

Carlson RC, Goldstein RH, Enos P. 2003. Effects of subaerial exposure on porosity evolution in the Carboniferous Lisburne Group, northeastern Brooks Range, Alaska, USA. AAPG Memoir, 269–290. doi: 10.2110/pec.03.78.0269.

Chen DZ, Tucker ME. 2003. The Frasnian-Famennian mass extinction: Insights from high-resolution sequence stratigraphy and cyclostratigraphy in South China. Palaeogeography, Palaeoclimatology, Palaeoecology, 193, 87–111. doi: 10.1016/S0031-0182(02)00716-2.

Chen DZ, Tucker ME, Jiang M, Zhu J. 2001. Long-distance correlation between tectonic-controlled, isolated carbonate platforms by cyclostratigraphy and sequence stratigraphy in the Devonian of South China. Sedimentology, 48, 57–78. doi: 10.1111/j.1365-3091.2001.00351.x.

Chen YQ, Zhou XY, Jiang SY, Zhao KD. 2013. Types and origin of dolostones in Tarim Basin, Northwest China: Petrographic and geochemical evidence. Acta Geologica Sinica-English Edition, 87, 467–485. doi: 10.1111/1755-6724.12062.

Chen YQ, Zhou XY, Yang HJ. 2010. Sequence stratigraphy and its control on burial karstification dolostone reservoir in the upper Cambrian Xiaqiulitage Formation at Xiao 'erbu lake section,Tarim basin. Journal of Stratigraphy, 34, 77–82 (in Chinese with English abstract). doi: 10.1017/S0004972710001772.

Chen ZQ, Shi GR. 2003. Late Paleozoic depositional history of the Tarim basin, northwest China: An integration of biostratigraphic and lithostratigraphic constraints. AAPG Bulletin, 87, 1323–1354. doi: 10.1306/0401032001115.

Choquette PW, Cox A, Meyers WJ. 1992. Characteristics, distribution and origin of porosity in shelf dolostones: Burlington-Keokuk Formation (Mississippian), US mid-continent. Journal of Sedimentary Research, 62, 167–189. doi: 10.1306/D42678B6-2B26-11D7-8648000102C1865D.

Choquette PW, Pray LC. 1970. Geologic nomenclature and classification of porosity in sedimentary carbonates. AAPG Bulletin, 54, 207–250. doi: 10.1016/0029-8018(69)90006-7.

Dickson J, Saller AH. 1995. Identification of subaerial exposure surfaces and porosity preservation in Pennsylvanian and Lower Permian shelf limestones, eastern Central Basin platform, Texas. AAPG Memoir, 63, 239–257.

Dong SF, Chen DZ, Qing HR, Zhou XQ, Wang D, Guo ZH, Jiang MS, Qian YX. 2013. Hydrothermal alteration of dolostones in the Lower Ordovician, Tarim Basin, NW China: Multiple constraints from petrology, isotope geochemistry and fluid inclusion microthermometry. Marine and Petroleum Geology, 46(3), 270–286. doi: 10.1016/j.marpetgeo.2013.06.013.

Dong SF, Chen DZ, Zhou XQ, Qian YX, Tian M, Qing HR. 2017. Tectonically driven dolomitization of Cambrian to Lower Ordovician carbonates of the Quruqtagh area, north-eastern flank of Tarim Basin, north-west China. Sedimentology, 64, 1079–1106. doi: 10.1111/sed.12341.

Eichenseer HT, Walgenwitz FR, Biondi PJ. 1999. Stratigraphic control on facies and diagenesis of dolomitized oolitic siliciclastic ramp sequences (Pinda Group, Albian, offshore Angola). AAPG Bulletin, 83, 1729–1758. doi: 10.2118/59476-PA.

Esteban M, Wilson JL. 1993. Introduction to karst systems and paleokarst reservoirs, in RD Fritz, JL Wilson, DA Yurewicz, (eds.), Paleokarst related hydrocarbon reservoirs. SEPM Core Workshop, 18, 1–10.

Fan TL, Yu BS, Gao ZQ. 2007. Characteristics of carbonate sequence stratigraphy and its control on oil-gas in Tarim Basin. Geoscience, 21, 57–65 (in Chinese with English abstract). doi: 10.1016/S1872-5813(07)60034-6.

Feng ZZ, Bao ZD, Wu MB, Jin ZK, Shi XZ. 2007. Lithofacies palaeogeography of the Cambrian in Tarim area. Frontiers of Earth Science in China, 1, 265–274. doi: 10.1007/s11707-007-0033-2.

Fischer AG. 1964. The Lofer cyclothems of the alpine Triassic, in: Merriam DF (ed.), Symposium on cyclic sedimentation: Kansas state geological survey bulletin 169, 107–149.

Goldhammer R, Dunn P, Hardie L. 1990. Depositional cycles, composite sea-level changes, cycle stacking patterns, and the hierarchy of stratigraphic forcing: Examples from Alpine Triassic platform carbonates. Geological Society of America Bulletin, 102, 535–562. doi: 10.1130/0016-7606(1990)1022.3.CO;2.

Goldhammer RK, Dunn PA, Hardie L. 1987. High frequency glacio-eustatic sealevel oscillations with Milankovitch characteristics recorded in Middle Triassic platform carbonates in northern Italy. American Journal of Science, 287, 853–892. doi: 10.2475/ajs.287.9.853.

Gu JY. 2000. Characteristics and origin analysis of dolomite in lower Ordovician of Tarim Basin. Xinjiang Petroleum Geology, 21, 120–122 (in Chinese with English abstract).

Guo C, Chen DZ, Qing HR, Zhou XQ, Ding Y. 2020. Early dolomitization and recrystallization of the Lower-Middle Ordovician carbonates in western Tarim Basin (NW China). Marine and Petroleum Geology, 111, 332–349. doi: 10.1016/j.marpetgeo.2019.08.017.

Guo C, Chen DZ, Song YF, Zhou XQ, Ding Y, Zhang GJ. 2018a. Depositional environments and cyclicity of the Early Ordovician carbonate ramp in the western Tarim Basin (NW China). Journal of Asian Earth Sciences, 158, 29–48. doi: 10.1016/j.jseaes.2018.02.006.

Guo C, Chen DZ, Zhou XQ, Ding Y, Wei WW, Zhang GJ. 2018b. Depositional facies and cyclic patterns in a subtidal-dominated ramp

during the Early-Middle Ordovician in the western Tarim Basin (NW China). Facies, 64, 16. doi: 10.1007/s10347-018-0529-0.

Haq BU, Schutter SR. 2008. A chronology of Paleozoic sea-level changes. Science, 322, 64–68. doi: 10.1126/science.1161648.

Hu MY. 1993. Diagenesis and porosity evolution of Cambrian carbonate rock in the North Tarim Basin. Journal of Jianghan Petroleum Institute, 15, 1–8 (in Chinese with English abstract).

Hu MY, Ngia NR, Gao D. 2019. Dolomitization and hydrotectonic model of burial dolomitization of the Furongian-Lower Ordovician carbonates in the Tazhong Uplift, central Tarim Basin, NW China: Implications from petrography and geochemistry. Marine and Petroleum Geology, 106, 88–115. doi: 10.1016/j.marpetgeo.2019.04.018.

Huang HP, Zhang SC, Su J. 2016. Palaeozoic oil–source correlation in the Tarim Basin, NW China: A review. Organic Geochemistry, 94, 32–46. doi: 10.1016/j.orggeochem.2016.01.008.

Huang WH, Wang AJ, Wan H, Fan TL, Yu BS. 2012. Discussion on characteristics of the Cambrian-Ordovician carbonate rocks reservoirs and origin of dolostones in Tarim Basin. Journal of Palaeogeography, 14, 197–208 (in Chinese with English abstract). doi: 10.1007/s11783-011-0280-z.

James NP, Choquette PW. 1984. Diagenesis 9: Limestones-The meteoric diagenetic environment. Geoscience Canada, 11, 161–191. doi: 10.1029/SC004p0045.

James NP, Choquette PW. 1988. Paleokarst. Springer, 416. doi: 10.1007/978–1-4612–3748-8.

Jia CZ. 1997. Tectonic Characteristics and Petroleum, Tarim Basin, China. Beijing, Petroleum Industry Press (in Chinese).

Jia CZ, Wei GQ. 2002. Structural characteristics and petroliferous features of Tarim Basin. Chinese Science Bulletin, 47, 1–11. doi: 10.1007/BF02902812.

Jia CZ, Zhang SB, Wu SZ. 2004. Stratigraphy of the Tarim Basin and Adjacent Areas. Beijing, Science Press, 1063 (in Chinese).

Kang YZ, Kang ZH. 1996. Tectonic evolution and oil and gas of Tarim basin. Journal of Southeast Asian Earth Sciences, 13, 317–325. doi: 10.1016/0743-9547(96)00038-4.

Li DS, Liang DG, Jia CZ, Wang G, Wu QZ, He DF. 1996. Hydrocarbon accumulations in the Tarim basin, China. AAPG Bulletin, 80, 1587–1603. doi: 10.1371/journal.pone.0057536.

Lin CS, Yang HJ, Liu JY, Rui ZF, Cai ZZ, Li ST, Yu BS. 2011. Sequence architecture and depositional evolution of the Ordovician carbonate platform margins in the Tarim Basin and its response to tectonism and sea-level change. Basin Research, 24, 1–24. doi: 10.1111/j.1365-2117.2011.00536.x.

Lindsay RF, Kendall CGSC. 1985. Depositional Acies, Diagenesis, and Reservoir Character of Mississippian Cyclic Carbonates in the Mission Canyon Formation, Little Knife Field, Williston Basin, North Dakota, Carbonate Petroleum Reservoirs. Springer, 175 – 190. doi: 10.1007/978–1-4612–5040-1_11.

Liu JD, Tian JC, Zhang X, Xu M, Meng WB, Lin XB, Yang YJ, Li HW. 2009. Characteristics and petroleum geologic significances of the sequence boundary surfaced of Cambrian strata in Tarim Basin. Journal of Mineralogy and Petrology, 29, 1–6 (in Chinese with English abstract).

Loucks RG, Sarg JF. 1993. Carbonate Sequence Stratigraphy: Recent Developments and Applications-Includes Map. AAPG Mem, 515. doi: 10.1306/M57579.

Lucia F, Major R. 1994. Porosity evolution through hypersaline reflux dolomitization. Dolomites: A Volume in Honour of Dolomieu, 67, 325–341. doi: 10.1002/9781444304077.ch18.

Mazzullo S, Harris P. 1992. Mesogenetic dissolution: Its role in porosity development in carbonate reservoirs. AAPG Bulletin, 76, 607–620. doi: 10.1029/92GL00942.

Moore CH. 1989. Carbonate Diagenesis and Porosity. Elsevier Science, 338.

Moore CH. 2001. Carbonate Reservoirs: Porosity Evolution and Diagenesis in A Sequence Stratigraphic Framework. Elsevier Science, 444.

Moore CH, Wade WJ. 2013. Carbonate Reservoirs: Porosity and Diagenesis in A Sequence Stratigraphic Framework. Elsevier, 369.

Ngia NR, Hu MY, Gao D. 2019. Tectonic and geothermal controls on dolomitization and dolomitizing fluid flows in the Cambrian-Lower Ordovician carbonate successions in the western and central Tarim Basin, NW China. Journal of Asian Earth Sciences, 172, 359–382. doi: 10.1016/j.jseaes.2018.09.020.

Osleger D, Read JF. 1993. Comparative analysis of methods used to define eustatic variations in outcrop: Late Cambrian interbasinal sequence development. American Journal of Science, 293, 157–216. doi: 10.2475/ajs.293.3.157.

Purser B, Brown A, Aissaoui D. 1994. Nature, origins and evolution of porosity in dolomites. in Purser B, Tucker M, Zenger D, (eds.), Dolomites: International association of sedimentologists Special Publication 21, 281–308.

Read J, Goldhammer R. 1988. Use of Fischer plots to define third-order sea-level curves in Ordovician peritidal cyclic carbonates, Appalachians. Geology, 16, 895–899. doi: 10.1130/0091-7613(1988)0162.3.CO;2.

Read J, Horbury AD. 1993. Eustatic and tectonic controls on porosity evolution beneath sequence-bounding unconformities and parasequence disconformities on carbonate platforms. AAPG Special Publication, 36, 155–197. doi: 10.1109/TC.2016.2515170.

Saller AH, Dickson J, Boyd SA. 1994. Cycle stratigraphy and porosity in Pennsylvanian and Lower Permian shelf limestones, eastern Central Basin Platform, Texas. AAPG Bulletin, 78, 1820–1842. doi: 10.1016/0022-1694(94)90149-X.

Saller AH, Dickson J, Matsuda F. 1999a. Evolution and distribution of porosity associated with subaerial exposure in upper Paleozoic platform limestones, west Texas. AAPG Bulletin, 83, 1835–1854. doi: 10.1306/E4FD4279-1732-11D7-8645000102C1865D.

Saller AH, Dickson J, Rasbury E, Ebato T. 1999b. Effects of long-term accommodation change on short-term cycles, upper Paleozoic platform limestones, West Texas. Advances in carbonate sequence stratigraphy: Application to reservoirs, outcrops and models, SEPM Special Publication, 63, 227–246.

Saller AH, Henderson N. 1998. Distribution of porosity and permeability in platform dolomites: Insight from the Permian of west Texas. AAPG Bulletin, 82, 1528–1550. doi: 10.1016/S0377-0273(98)00026-2.

Saller AH, Lounsbury K, Birchard M. 2001. Facies control on dolomitization and porosity in the Devonian Swan Hills Formation in the Rosevear area, west-central Alberta. Bulletin of Canadian Petroleum Geology, 49, 458–471. doi: 10.2113/49.4.458.

Sarg J. 1988. Carbonate sequence stratigraphy, in Wilgus CK, Hastings BS, Kendall CG St C, Posamentier HW, Ross CA, Wagoner Van JC, (eds.), Sea-Level Changes: An Integrated Approach. SEPM, Special Publication, 42, 155–181.

Shao LW, He H, Peng SP, Li RJ. 2002. Types and origin of dolostones of the Cambrian and Ordovician of Babu uplift area in Tarim Basin. Journal of paleogeography, 4, 19–30 (in Chinese with English abstract).

Shen AJ, Zheng JF, Pan WQ, Zhang LJ, Zheng XP, Luo XY. 2009. Types and the characteristics of Lower Paleozoic dolostone reservoirs in Tarim Basin. Marin Origin Petroleum Geology, 14, 1–9 (in Chinese with English abstract).

Sibley DF, Gregg JM. 1987. Classification of dolomite rock textures. Journal of Sedimentary Research, 57, 967–975.

Stemmerik L, Larssen GB. 1993. Diagenesis and porosity evolution of Lower Permian Palaeoaplysina build-ups, Bjørnøya: An example of

diagenetic response to high frequency sea level fluctuations in an arid climate. AAPG Special Publication, 36, 199–211.

Sun SQ. 1995. Dolomite reservoirs: Porosity evolution and reservoir characteristics. AAPG Bulletin, 79, 186–204. doi: 10.1306/8D2B14EE-171E-11D7-8645000102C1865D.

Tang LJ. 1997. Major evolutionary stages of Tarim Basin in Phanerozoic time. Earth Science Frontiers, 4, 318–324 (in Chinese with English abstract).

Tucker ME. 1993. Carbonate diagenesis and sequence stratigraphy, in: Wright VP (ed.), Sedimentology Review/1. Oxford, Blackwell Scientific Publications, 51–72.

Tucker ME, Wright VP, Dickson J. 1990. Carbonate Sedimentology. Wiley-Blackwell, 482.

Wang XL, Lin CS, Jiao CL, Huang LL. 2018. Dolomite reservoir types and development models of Middle-Upper Cambrian in Tarim Basin. Lithologic Reservoirs, 30, 63–74 (in Chinese with English abstract).

Xiao ZH, Wang ZM, Jiang RQ, Wu JC, Zhang LJ. 2011. Sequence stratigraphic features of the Cambrian carbonate rocks in the Tarim Basin. Oil & Gas Geology, 32, 1–10 (in Chinese with English abstract).

Yang YJ, Liu JD. 2011. Sequence lithofacies paleogeography of Cambrian in Tarim Basin. Natural Gas Geoscience, 22, 450–459 (in Chinese with English abstract).

Ye DS. 1992. The origin of the Qiulitage Group dolomite (Cambrian to Ordovician) in northern Tarim Basin. Acta Sedimentologica Sinica, 10, 77–86 (in Chinese with English abstract).

Ye DS. 1994. Deep dissolution of Cambrian-Ordivician carbonates in the Northern Tarim Basin. Acta Geologica Sinica, 12, 66–71 (in Chinese with English abstract).

You X, Sun S, Zhu J, Li Q, Hu W, Dong H. 2013. Microbially mediated dolomite in Cambrian stromatolites from the Tarim Basin, north-west China: Implications for the role of organic substrate on dolomite precipitation. Terra Nova, 25, 387–395. doi: 10.1111/ter.12048.

Yu BS, Chen JQ, Lin CS. 2005. Sequence stratigraphid framework and its control on development of Ordovician carbonate reservoir in Tarim Basin. Oil & Gas Geology, 26, 305–316 (in Chinese with English abstract).

Yu BS, Fan TL, Huang WH, Liu ZB, Gao ZQ. 2007. Predictive model for karst reservoirs in sequence stratigraphic framework. Acta Petrolei Sinica, 28, 41–45 (in Chinese with English abstract).

Zhang JT, Hu WX, Qian YX, Wang XL, Xie XM. 2008. Classification and logging modes of the dolomite reservoirs in Tarim basin, NW China. Acta Geologica Sinica, 82, 380–386 (in Chinese with English abstract).

Zhang SB, Gao QQ. 1992. Sinian to Permian Stratigraphy and Palaeontology of the Tarim Basin, Xinjiang, II, Kalpin-Bachu Region. Beijing, The Petroleum Industry Press, 329 (in Chinese with English abstract).

Zhang YQ, Chen DZ, Zhou XQ, Guo ZH, Wei WW, Mutti M. 2015. Depositional facies and stratal cyclicity of dolomites in the Lower Qiulitag Group (Upper Cambrian) in northwestern Tarim Basin, NW China. Facies, 61, 1–24. doi: 10.1007/s10347-014-0417-1.

Zhang ZY, Zhu GY, Zhang YJ, Han JF, Li TT, Wang E, Greenwood P. 2018. The origin and accumulation of multi-phase reservoirs in the east Tabei uplift, Tarim Basin, China. Marine and Petroleum Geology, 98, 533–553. doi: 10.1016/j.marpetgeo.2018.08.036.

Zhao WZ, Shen AJ, Zheng JF, Qiao ZF, Wang XF, Lu JM. 2014. The porosity origin of dolostone reservoirs in the Tarim, Sichuan and Ordos basins and its implication to reservoir prediction. Science China Earth Sciences, 57, 2498–2511. doi: 10.1007/s11430-014-4920-6.

Zheng HR, Wu MB, Wu XW, Zhang T, Liu CY. 2007. Oil-gas exploration prospect of dolomite reservoir in the Lower Paleozoic of Tarim Basin. Acta Petrolei Sinica, 28, 1–8 (in Chinese with English abstract). doi: 10.1111/j.1745-7254.2007.00491.x.

Zheng JF, Shen AJ, Chen YQ, Ni X, Zhang XL. 2015. Reservoir space and reservoir classificantion of Lower Paleozoic dolomite in the Tarim Basin. Natural Gas Geoscience, 26, 1256–1267. doi: 10.11764/j.issn.1672-1926.2015.07.1256.

Zheng JF, Shen AJ, Liu YF, Chen YQ. 2012. Multi-parameter comprehensive identification of the genesis of Lower Paleozoic dolomite in Tarim Basin, China. Acta Petrolei Sinica, 33, 145–153 (in Chinese with English abstract). doi: 10.1038/aps.2011.185.

Zhou LK, Zhou TR, Wang P, Jia RX. 1991. Age of Qiulitag Group in NE Tarim Basin. In: Jia RX (ed.), Research of petroleum geology of northern Tarim basin in China: Stratigraphy sedimentology. China University of Geosciences, Wuhan, 36–40 (in Chinese).

Zhou XQ, Chen DZ, Dong SF, Zhang YQ, Guo ZH, Wei HY, Yu H. 2015. Diagenetic barite deposits in the Yurtus Formation in Tarim Basin, NW China: Implications for barium and sulfur cycling in the earliest Cambrian. Precambrian Research, 263, 79–87. doi: 10.1016/j.precamres.2015.03.006.

Zhou XQ, Chen DZ, Qing HR, Qian YX, Wang D. 2014. Submarine silica-rich hydrothermal activity during the earliest Cambrian in the Tarim Basin, Northwest China. International Geology Review, 56, 1906–1918. doi: 10.1080/00206814.2014.968885.

Zhou ZY. 2001. Stratigraphy of the Tarim Basin. Beijing, Science Press, 359 (in Chinese with English abstract).

Zhou ZY, Chen PJ, Wang YJ. 1990. Biostratigraphy and Geology Evolution in Tarim Basin. Beijing, Science Press, 399 (in Chinese).

Zhu DY, Meng QQ, Jin ZJ, Liu QY, Hu WX. 2015. Formation mechanism of deep Cambrian dolomite reservoirs in the Tarim basin, northwestern China. Marine and Petroleum Geology, 59, 232–244. doi: 10.1016/j.marpetgeo.2015.12.020.